



Sandstones of the Itmurundy accretionary complex, central Kazakhstan, as archives of arc magmatism and subduction erosion: Evidence from U-Pb zircon ages, geochemistry and Hf-Nd isotopes

Inna Safonova^{a,b}, Alina Perfilova^{a,c,*}, Ilya Savinskiy^a, Pavel Kotler^{a,c}, Min Sun^d, Bo Wang^e

^a Novosibirsk State University, Pirogova St. 1, Novosibirsk 630090, Russia

^b Zavaritskiy Institute of Geology and Geochemistry, UrB RAS, Vonsovskogo ave. 15, Yekaterinburg 620016, Russia

^c Sobolev Institute of Geology and Mineralogy, SB RAS, Koptyuga ave. 3, Novosibirsk 630090, Russia

^d Department of Earth Sciences, the University of Hong Kong, Pokfulam, Road, Hong Kong, China

^e State Key Laboratory for Mineral Deposits Research, Department of Earth Sciences, Nanjing University, Nanjing 210093, China

ARTICLE INFO

Article history:

Received 21 April 2022

Revised 20 June 2022

Accepted 29 June 2022

Available online 10 July 2022

Handling Editor: M. Santosh

Keywords:

Paleo-Asian Ocean

Central Asian Orogenic Belt

Ordovician-early Silurian

U-Pb-Hf zircon data

Greywacke sandstones

ABSTRACT

Sandstones hosted by Pacific-type orogenic belts and related accretionary complexes carry records of their source intra-oceanic or continental magmatic arcs. Study of arc-derived sandstones is important for reconstructing tectonic evolution of Pacific-type convergent margins in case such arcs get partly or completely eroded during subduction. In this paper, we present first U-Pb detrital zircon ages and Hf-in-zircon isotope ratios and whole-rock geochemical and Nd data from Ordovician to early Silurian clastic sediments (sandstones) of the Itmurundy Pacific-type orogenic belt and its hosted accretionary complex (AC). The Itmurundy AC is located in the northern Balkhash area of central Kazakhstan and includes sandstones of the Itmurundy and Kazyk fms. (central segment) and Tyuretai Fm. (eastern segment). The U-Pb ages of detrital zircons from Group 1 sandstones show unimodal distributions with major peaks at ca. 467–456 Ma and the youngest clusters of ages from 442 to 439 Ma suggesting post-Llandovery deposition. The distributions of the U-Pb ages of detrital zircons from Group 2 sandstones are polymodal with major peaks at ca. 462–461 Ma and subordinate peaks at 788, 992, 2472 Ma. The Group 2 zircons yielded two youngest clusters of U-Pb ages: 458 Ma and 424 Ma suggesting post-middle Ordovician and post-Ludlow maximum depositional ages. According to petrographic classifications, both Group 1 and 2 sandstones are poorly-sorted and poorly-rounded greywacke or litharenite. The chemical compositions imply that these sandstones are immature and weakly weathered sediments. The Group 1 greywackes are characterized by relatively low SiO₂ (63 wt%) compared to Group 2 greywackes (SiO₂ = 66 wt% in average). The major and trace element compositions of both groups of sandstones resemble those of supra-subduction andesitic to dacitic volcanic rocks. The positive values of whole-rock $\epsilon_{\text{Nd}}(t)$ (+1 to +5.3) and zircon $\epsilon_{\text{Hf}}(t)$ (+9.8 to +17.5) obtained from the Group 1 greywackes suggest juvenile igneous rocks in the source area. On the contrary, the negative values of $\epsilon_{\text{Nd}}(t)$ (–7.2) and variable values of zircon $\epsilon_{\text{Hf}}(t)$ (–24.5 to +11.5) from the Group 2 sandstones suggest that their parental igneous rocks were derived from mantle sources possessing both juvenile and recycled characteristics. Conclusively, the greywacke sandstones of both groups formed by erosion of an Ordovician intra-oceanic volcanic arc once existed at an active margin of the Paleo-Asian Ocean, however those of Group 1 deposited in a fore-arc basin and trench, while those of Group 2 deposited in a back-arc basin.

© 2022 International Association for Gondwana Research. Published by Elsevier B.V. All rights reserved.

1. Introduction

Pacific-type orogenic belts record evolution of oceans from their opening to their closure and therefore their study is of key importance for understanding the global geological history of the Earth. Pacific-type orogens host supra-subduction and accretionary complexes, which are archives of subduction zone magmatism and ocean plate stratigraphy (Khanchuk et al., 1989; Isozaki et al.,

* Corresponding author at: Novosibirsk State University, Pirogova St. 1, Novosibirsk 630090, Russia.

E-mail addresses: inna03-64@mail.ru (I. Safonova), alinalopolina@gmail.com (A. Perfilova).

1990; Maruyama, 1997). Supra-subduction complexes consist of intra-oceanic arc and continental arc-related igneous units and fore-arc and back-arc sedimentary deposits. Accretionary complexes include both fragments of oceanic crust detached from subducting oceanic plate, as well as material coming from adjacent magmatic arcs (e.g., Isozaki et al., 1990; Maruyama, 1997; Wakita and Metcalfe, 2005; Safonova, 2009; Kusky et al., 2013).

At modern Pacific-type convergent margins, supra-subduction and accretionary complexes are tens to hundreds kilometers apart. In the process of ocean suturing, the supra-subduction and accretionary complexes can be spatially juxtaposed. The destruction of supra-subduction magmatic arcs and the delivery of eroded material into fore-arc trough and/or into trench form characteristic clastic sedimentary rocks: greywacke sandstones and turbidites. Their study is critical for paleotectonic reconstructions in case those magmatic arcs get partially or even completely destroyed by surface and subduction erosion and therefore disappear from the geological record (e.g., Ueda et al., 2000; Clift and Vannucchi, 2004; Scholl and von Huene, 2007). Unlike magmatic arcs, greywacke and turbidite sandstones typically remain on the surface, allowing us to determine the nature of a former magmatic arc, intra-oceanic versus continental. Sandstones often contain detrital zircons, which age typically reflects the age of igneous rocks in the source area and which Hf-in-zircon isotopes characterize a type of their source – juvenile or recycled. The turbidites and greywackes related to intra-oceanic subduction zones are compositionally (bulk) similar to their parental igneous rocks (typically mafic to andesitic), and the age of zircons reflects the age of island arc. On the contrary, the sandstones formed at continental arcs are compositionally more felsic and may carry detrital zircons older than the associated supra-subduction igneous rocks (typically andesitic to dacitic). Reconstruction of sources and tectonic settings of deposition of clastic sediments, first of all sandstones, hosted by accretionary complexes, requires detailed geological, geochronological (U-Pb detrital zircon ages), geochemical and isotope studies (e.g., Dickinson and Suczek, 1979; Bhatia and Crook, 1986; Zhang, 2004; Long et al., 2010, 2012).

Accretionary complexes compose a major part of the Central Asian Orogenic Belt (CAOB) the world largest intracontinental Phanerozoic accretionary orogen formed by the evolution and suturing of the Paleo-Asian Ocean (PAO) (e.g., Zonenshain et al., 1990; Buslov et al., 2001; Jahn, 2004; Windley et al., 2007; Kröner et al., 2007, 2014; Safonova, 2009). The CAOB is a collage of Pacific-type orogens as it hosts numerous intra-oceanic arcs with juvenile crust, accretionary and blueschist complexes (e.g., Jahn, 2004; Windley et al., 2007; Xiao et al., 2010, 2020; Safonova et al., 2017, 2018). On the other hand, the CAOB includes numerous microcontinents with Precambrian isotopically recycled crust. Consequently, the nature of the CAOB crust, juvenile vs recycled, remains a matter of debates (Kröner et al., 2014, 2017; Safonova et al., 2011; Safonova, 2017). A reason for such a discrepancy is probable subduction erosion of island arcs consisting of igneous complexes with juvenile isotopic characteristics as the disappearance of arcs could have shifted the balance between the juvenile and recycled crust to the latter resulting in biased interpretations (Safonova, 2017; Safonova et al., 2021; Konopelko et al., 2021).

The Itmurundy Pacific-type orogenic belt is located in the Itmurundy zone in the western CAOB (Figs. 1, 2, S1). The Itmurundy zone includes a Pacific-type orogenic belt consisting of accretionary complex and adjacent ophiolite belt (Safonova et al., 2019, 2020) and younger post-orogenic formations and granitoids (Fig. 2). The ophiolite belt and accretionary complex formed at an early Paleozoic stage of PAO evolution (Safonova et al., 2019). It has been studied by many scientists, but mostly for geology and micropaleontology (Patalakha and Belyi, 1981; Novikova et al.,

1983; Zhylkaidarov, 1998; Nikitin, 2002). Recently, there have been published first U-Pb zircon ages (plagiogranites and diorites) and first high-precision geochemical and isotope data from volcanic rocks (Stepanets, 2016; Safonova et al., 2020; Degtyarev et al., 2020b, 2021a). However, the amount of such data remain limited and the outcrops of arc-related volcanic rocks are small and sheared, and their age remains enigmatic. Therefore, up-to-date geochronological and geochemical/isotope data from sedimentary clastic rocks, i.e., sandstones of supra-subduction and accretionary units, are of crucial importance for developing a coherent tectonic model for the Itmurundy orogenic belt.

In this paper, we present petrographic, geochronological, and geochemical data, including first U-Pb detrital zircon ages, Hf-in-zircon, and whole-rock Nd isotopic data from clastic sediments (sandstones) of the Itmurundy AC. Our results provide new constraints on the provenance of the sandstones, depositional tectonic settings and parental igneous rocks. The obtained data from those clastic rocks in combination with the previous data from Itmurundy igneous formations and from adjacent coeval formations of western Junggar in NW China will definitely contribute to the better understanding of the complex tectonic evolution of the western CAOB.

2. Geological framework

2.1. The Itmurundy belt and accretionary complex

The Itmurundy Pacific-type orogenic belt of the Itmurundy zone extends over a distance more than 80 km along Lake Balkhash (Fig. 2, supplementary figure S1). It is a part of the Junggar-Balkhash folded system located in central Kazakhstan and NE China (Fig. 1). The Itmurundy belt consists of tectonic sheets and slivers of early Paleozoic ophiolites, accretionary complex, metamorphic belt, and mélangé including sedimentary and igneous rocks separated by faults (Patalakha and Belyi, 1981; Safonova et al., 2019). The geological units of Cambrian to early Silurian age (Fig. 2) belong to the Itmurundy Pacific-type orogenic belt or simply Itmurundy belt (Safonova et al., 2019). The Ludlow to Viséan units formed in a different tectonic setting (post-orogenic). The Itmurundy accretionary complex (AC) includes the full set of Ocean Plate Stratigraphy (OPS) lithologies: MORB and OIB-type basalts, pelagic oceanic sediments (ribbon chert) and hemipelagic sediments (siliceous siltstone, shale, mudstone) and turbidite. In addition, there are numerous beds of greywacke sandstone of unclear tectonic origin (Safonova et al., 2020; Perfilova et al., 2022). Traditionally, the Itmurundy AC includes rocks of three main formations: Itmurundy (O₁₋₂), Kazyk (O₂₋₃) and Tyuretai (O_{3-S1}) (Koshkin and Galitskiy, 1960; Patalakha and Belyi, 1981) outcropping in the central and eastern part of the belt (Figs. 2, 3). The oldest Itmurundy Fm. is dominated by basaltic lavas with subordinate cherts and siliceous mudstone. The Early-Middle Ordovician age of the Itmurundy Fm. is constrained by conodonts hosted by chert (Novikova et al., 1983; Degtyarev et al., 2020a) and siliceous mudstone (Degtyarev et al., 2020a). The Kazyk Fm. is dominated by pelagic ribbon chert and siliceous mudstone and siltstone with subordinate basalts and clastic sediments. The Middle-Late Ordovician age of the Kazyk Fm. is constrained by chert-hosted conodonts (Novikova et al., 1983; Safonova et al., 2019; Degtyarev et al., 2020a). The youngest Tyuretai Fm. consists of thick fine- to coarse-grained clastic sediments, sandstone and gravelstone, overlapping siliceous siltstone, mudstone, chert and volcanics. Evidence for the Late Ordovician – Early Silurian age of the Tyuretai Fm. comes also from chert-hosted conodonts (Novikova et al., 1983; Degtyarev et al., 2020a) and siltstone-hosted graptolites (Zhylkaidarov, 1998). A bit aside is the Djaman-

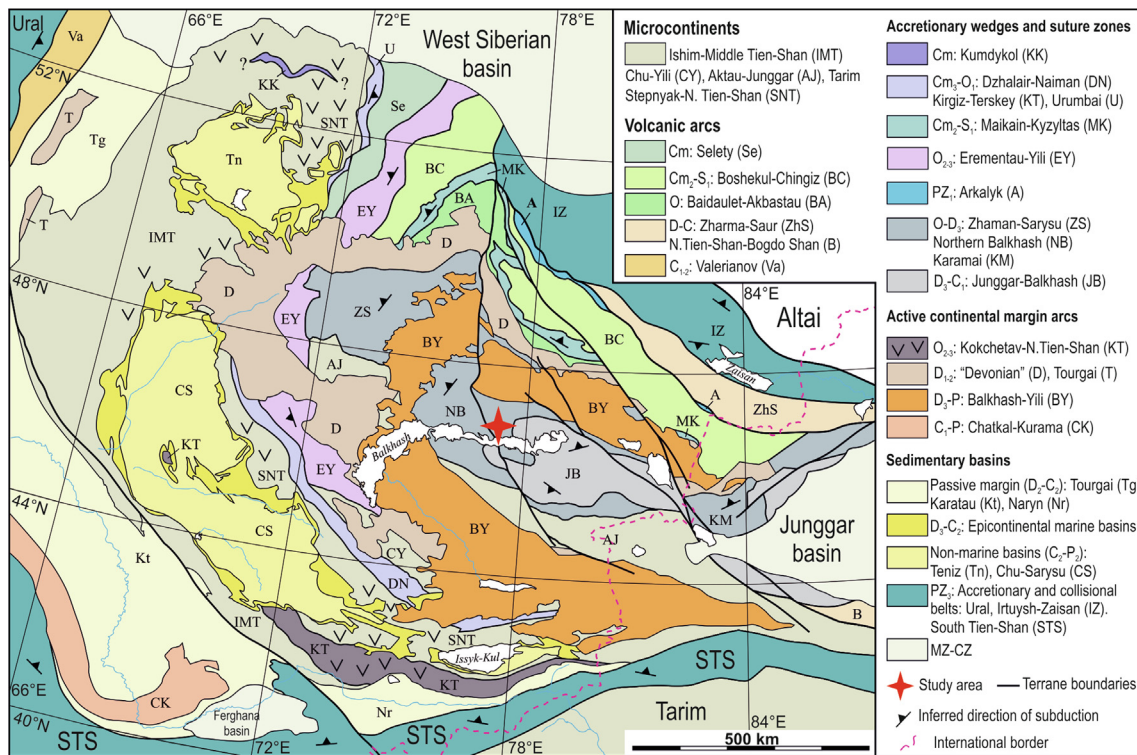


Fig. 1. Geotectonic map of the major Palaeozoic structures of Kazakhstan and adjacent regions of China, Kyrgyzstan and Uzbekistan (modified after Windley et al., 2007). Red star shows the location of the Itmurundy belt.

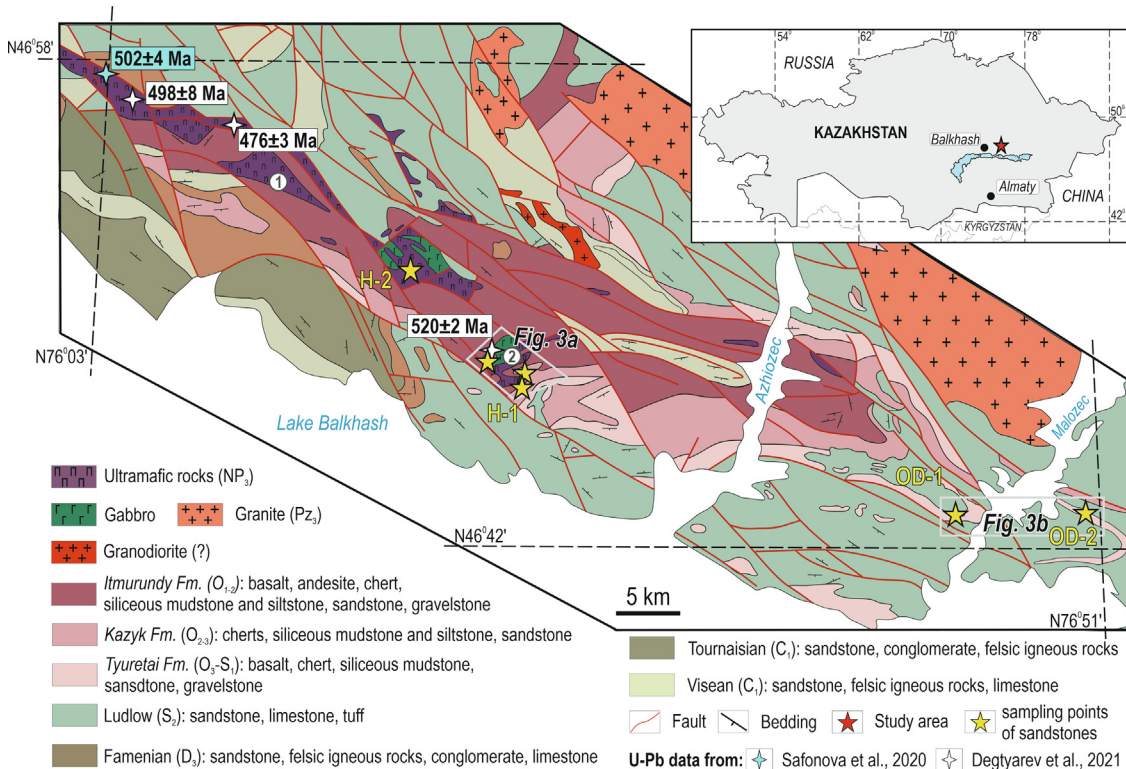


Fig. 2. An updated fragment of the 1/200 000 geological map of the Itmurundy zone based on the Geological map of the USSR, Sheet L-43-XI (Koshkin and Galitsky, 1960) and modified after (Safonova et al., 2020). Numbers in circles are for the Kentaralau (1) and East Arkharsu (2) ophiolite massifs. The Itmurundy zone includes orogenic and post-orogenic formations. The late Precambrian to early Silurian igneous complexes and sedimentary formations are constituents of the Itmurundy Pacific-type orogenic belt (Safonova et al., 2019). The Ludlow to Visean formations are post-orogenic.

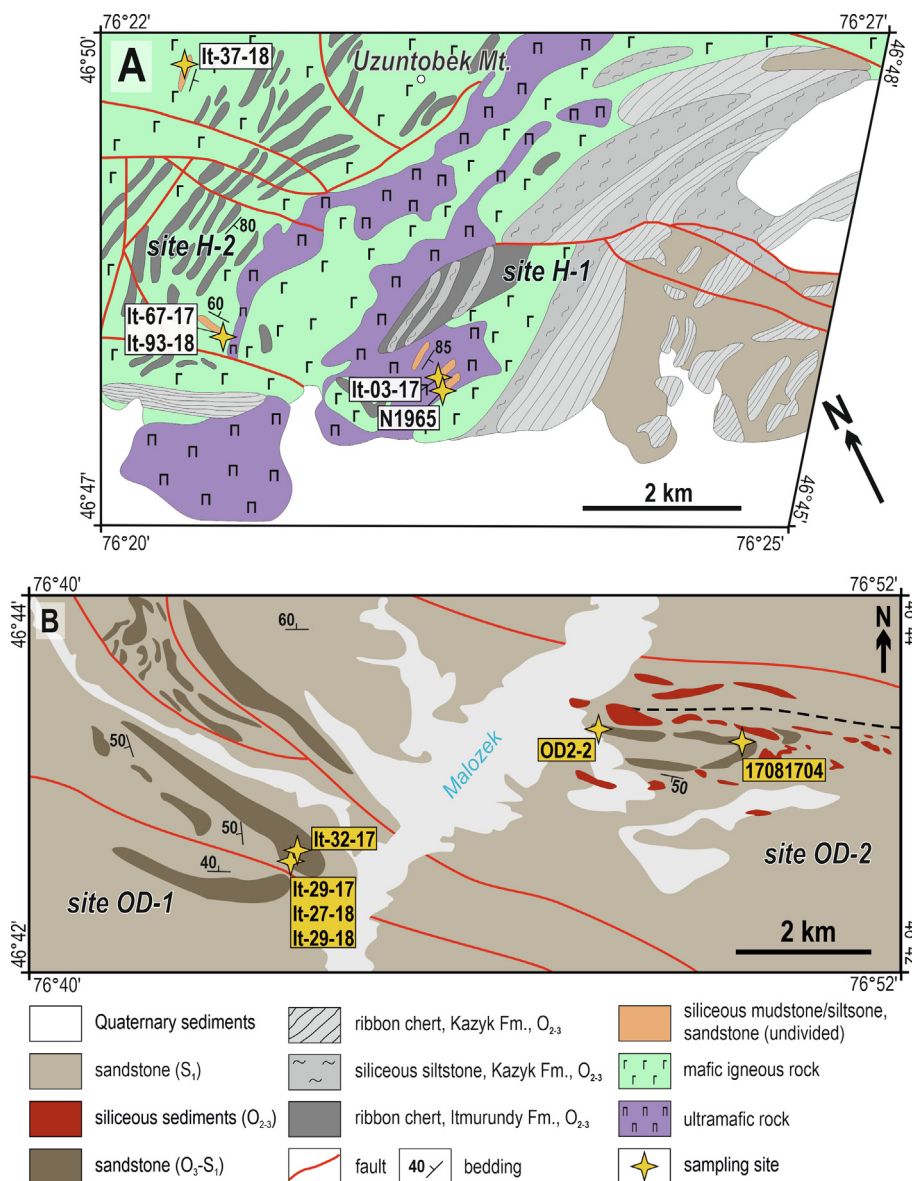


Fig. 3. Geological sketches of the study sites: a) H-1, H-2; b) OD-1, OD-2. The frames for each site are shown in Fig. 2. The schemes show the location of key samples only (for more details see Table 1).

shuruk Fm. (O₃) (Nikitin, 2002; Degtyarev et al., 2020) consisting of gravelstone, sandstone with tuff interbeds, mafic to andesitic volcanic rocks, and scarce limestone outcropped north of the Itmurundy belt (Patalakha and Belyi, 1981; Nikitin, 2002). The Middle-Late Ordovician age constrains of the Djmanshuruk Fm. come from brachiopods, trilobites and corals in limestones and conodonts in chert (Nikitin, 2002).

Later, other scientists recognized more formations, e.g., Ushbulak (O₂₋₃) and Obaly (O₃) (Degtyarev et al., 2020, 2021a). The Ushbulak Fm. crops out in the eastern part of the Itmurundy belt and is dominated by mafic to felsic volcanic rocks, tuff, and chert with Middle Ordovician conodonts (Degtyarev et al., 2020). The Obaly Fm. consists of clastic sediments and olistostrome with subordinate chert, siliceous siltstone and tuff cropping out in the northern part of the belt (Degtyarev et al., 2021a). Its Late Ordovician age was determined by conodonts in siliceous siltstone and mudstone (Degtyarev et al., 2020a). The newly recognized Ushbulak Fm. and Obaly Fm. overlap with the Itmurundy Fm. and the Tyuretai Fm., respectively, although their ages and lithologies are similar. Note

that accretionary complexes typically have duplexed structures and each tectonic sheet may contain microfauna of different or similar ages (e.g., Matsuda and Isozaki, 1991; Maruyama et al., 2010; Safonova et al., 2016). Therefore, it is practically useless to identify more and more formations at each new finding of microfauna or each new U-Pb zircon age while studying an accretionary complex. However, we would like to stress out that traditional stratigraphy, microfossils and U-Pb zircon ages are still very important, however, their direct application and interpretation remains problematic because OPS units in structurally complicated accretionary complexes often remain poorly reconstructed due to the lack of detailed structural analysis, first of all, duplexes (Maruyama et al., 2010; Wakita, 2012). The geological maps of Japanese Islands, which structure is dominated by accretionary complexes, never show such classical stratigraphic subdivisions as “formation” or “suite” in a traditional stratigraphic sense. They show units or domains separated from each other by major thrusts (e.g., Isozaki et al., 1990; Wakita, 2012; Safonova et al., 2016). Accordingly, in this paper for linking our samples to this or that

geological structure/entity, we prefer to use term “site” in a geology-based geographic sense rather than “formation” in a stratigraphic sense.

2.2. Sampling sites

We performed detailed fieldwork and collected samples of clastic sediments (Table 1) at four sites of the Itmurundy AC: sites H-1 and H-2 of the central segment (Group 1) and sites OD-1 and OD-2 of the eastern segment (Group 2) (Figs. 2, 3). Site H-1 is located in the central part of the Itmurundy AC (Figs. 2, 3A) and includes outcrops of basalt, often as pillow-lava, red ribbon chert, brown and greenish grey siliceous mudstones, fine-medium grained greenish grey sandstones, and volcanoclastic sediments (Fig. 3A, 4A). Site H-1 pelagic chert contains Middle Ordovician to early Late Ordovician conodonts and is considered to belong to the Kazyk Fm. (Novikova et al., 1983; Nikitin, 2002; Safonova et al., 2019; Degtyarev et al., 2020). The poorly sorted sandstones of site H-1 occur in the upper part of the section (Fig. 4A) and outcrop at small hills or are interbedded with hemipelagic sediments to form turbiditic packages (Fig. 5A, B). The thickness of sandstones ranges from 1 to 3 m.

Site H-2 is located in the north-western part of the Itmurundy AC (Figs. 2, 3A). The site is dominated by high-Ti basalts (Safonova et al., 2020) associated with chert and siliceous siltstones/mudstones with subordinate terrigenous sediments (Fig. 4B-F, 5C). Site H-2 sandstones also outcrop at hill summits and are associated with siliceous deep-marine sediments – brown and grey-green siliceous mudstones (Fig. 4C) and brown-red chert (Fig. 4E) and volcanoclastic rocks. In places, thick turbidite packages are overlapped by tuffs (Fig. 4F) and may carry 2–3 m long lenses of siliceous mudstones (Fig. 4C). Basalts including pillow-lavas typically occur at bottom parts of the sections (Fig. 4B, D, F) and as thin flows in the upper parts (Fig. 4C, E). In places, the sandstones carry lenses of breccia with basaltic matrix and fragments of chert and siliceous mudstone (Fig. 4B, D). The thickness of sandstones ranges from 1 to 15 m.

Sites OD-1 and OD-2 are located in the eastern part of the Itmurundy AC (Figs. 2, 3B). They both represent partly overturned syn-

clines consisting of basalt, deep-sea and clastic sediments. Site OD-2 is a low-hilly area, where basalt and deep-sea sediments are exposed in the inner parts and clastic sediments outcrop at the outer parts of the syncline (Fig. 3B). The deep-sea and clastic packages (Fig. 4G) are attributed to the Kazyk and Tyuretai formations, respectively. The OD-1 syncline structurally and lithologically strongly resembles the famous Inuyama syncline of the Mino accretionary complex in Japan, the world type locality of ocean plate stratigraphy or OPS (Matsuda and Isozaki, 1991; Safonova et al., 2016). The Site OD-1 sandstones form either large outcrops up to 15 m thick (Fig. 5D), or small exposures of sheared packages in dry valleys (Fig. 5E). In sections/outcrops, the sandstones are intercalated with sandy siltstone and siliceous mudstone (Fig. 4G). The size of grains increases up the section that is typical of turbidites.

Site OD-2 is a topographically flat area with few small hills. There are grey-greenish and brown mid- to coarse-grained sandstones (Fig. 5F) composing small hills and debris-like small outcrops. The sample under study (Fig. 3B) is a light-brown coarse-grained sheared sandstone occurring as a 5–10 cm thick bed hosted by brown quartzite or recrystallized chert or siliceous mudstone. The quartzite is cross-cut by numerous quartz veins suggesting strong deformation. The scarcity of good outcrops makes difficulties in the understanding of relationships between different lithologies.

We sampled sandstones at best outcrops available at each locality to avoid fractures filled by quartz and calcite and pieces experienced weathering and hydrothermal alteration. Then we chose most representative samples for petrography and analytical studies: U-Pb detrital zircon dating, geochemical analyses (major oxides and trace elements) and isotopic analyses (whole-rock powders for Nd and zircon mounts for Hf-in-zircon). For details on methods and analytical procedures see Suppl. Electr. materials.

3. Petrography

We selected 18 samples of sandstones from all four sites in the central (Group 1) and eastern (Group 2) segments of the Itmurundy AC (Figs. 2, 3), respectively, for petrographic characterization

Table 1
Location of sampled sandstones of the Itmurundy accretionary complex.

Sample no.	Rock type	Formation*	Site**	Geography***	Coordinates
<i>Group 1 (central segment)</i>					
It-03-17	fine/medium grained sandstone	Kazyk	H-1	4.5 km south of Uzuntobek Mt.	46°47'17.9"; 76°23'12.2"
H1-7/1	coarse-grained sandstone	Kazyk	H-1	4 km south-east of Uzuntobek Mt.	46°47'31.1"; 76°23'25.7"
It-09-18	fine-grained sandstone	Kazyk	H-1	4 km south-east of Uzuntobek Mt.	46°47'39.9"; 76°22'52.6"
It-25-18	fine/medium grained sandstone	Kazyk	H-1	4 km south-east of Uzuntobek Mt.	46°47'35.2"; 76°22'59.6"
N1956	fine-grained sandstone/turbidite	Kazyk	H-1	5.3 km south-east of Uzuntobek Mt.	46°46'53.1"; 76°23'10.2"
N1965	fine-grained sandstone	Itmurundy	H-2	4 km south-east of Ushatogan Mt.	46°50'50.2"; 76°18'12.5"
17081808	fine/medium-grained sandstone	Itmurundy	H-2	4.5 km east of Uzuntobek Mt.	46°49'49.4"; 76°18'32.9"
It-37-18	fine-grained sandstone	Itmurundy	H-2	1.2 km east of Uzuntobek Mt.	46°49'33.2"; 76°21'12.6"
It-67-17	fine/medium-grained sandstone/turbidite	Itmurundy	H-2	3.2 km south of Uzuntobek Mt.	46°48'00.4"; 76°21'47.1"
It-69-18	fine/medium-grained sandstone/turbidite	Itmurundy	H-2	3.2 km south of Uzuntobek Mt.	46°47'58.7"; 76°21'47.6"
It-75-18	fine/medium-grained sandstone	Itmurundy	H-2	3.2 km south of Uzuntobek Mt.	46°47'57.7"; 76°21'47.5"
It-83-18	fine/medium-grained sandstone	Itmurundy	H-2	3.2 km south of Uzuntobek Mt.	46°47'56.6"; 76°21'46.6"
It-87-18	fine-grained sandstone	Itmurundy	H-2	3.2 km south of Uzuntobek Mt.	46°47'56.3"; 76°21'47.2"
It-91-18	fine-grained sandstone/turbidite	Itmurundy	H-2	3.2 km south of Uzuntobek Mt.	46°47'56.3"; 76°21'47.2"
It-93-18	fine/medium-grained sandstone/turbidite	Itmurundy	H-2	3.2 km south of Uzuntobek Mt.	46°47'55.1"; 76°21'47.4"
It-101-18	fine-grained sandstone	Itmurundy	H-2	3 km south of Uzuntobek Mt.	46°48'02.6"; 76°21'55.1"
<i>Group 2 (eastern segment)</i>					
It-29-17	fine/medium-grained sandstone/turbidite	Tyuretai	OD-1	4.1 km south-east Koskyzyl Mt.	46°43'06.1"; 76°44'27.2"
It-32-17	fine/medium-grained sandstone/turbidite	Tyuretai	OD-1	4.1 km south-east Koskyzyl Mt.	46°43'08.7"; 76°44'29.7"
It-27-18	fine/medium-grained sandstone/turbidite	Tyuretai	OD-1	3.8 km south Koskyzyl Mt.	46°43'10.7"; 76°42'25.0"
It-29-18	fine/medium-grained sandstone/turbidite	Tyuretai	OD-1	4.1 km south-east Koskyzyl Mt.	46°43'10.7"; 76°42'25.0"
OD2-2	medium/coarse-grained sandstone	Tyuretai	OD-2	7.4 km south-east Koskyzyl Mt.	46°43'41.2"; 76°48'31.3"
17081704	medium/coarse-grained sandstone	Tyuretai	OD-2	9.8 km south-east Koskyzyl Mt.	46°43'21.2"; 76°50'22.9"

* - the names of formations are given after (Patalakha and Belyi, 1981); ** - see Fig. 2 for the location of sites; *** - see supplementary figure S1 for the geographic outline.

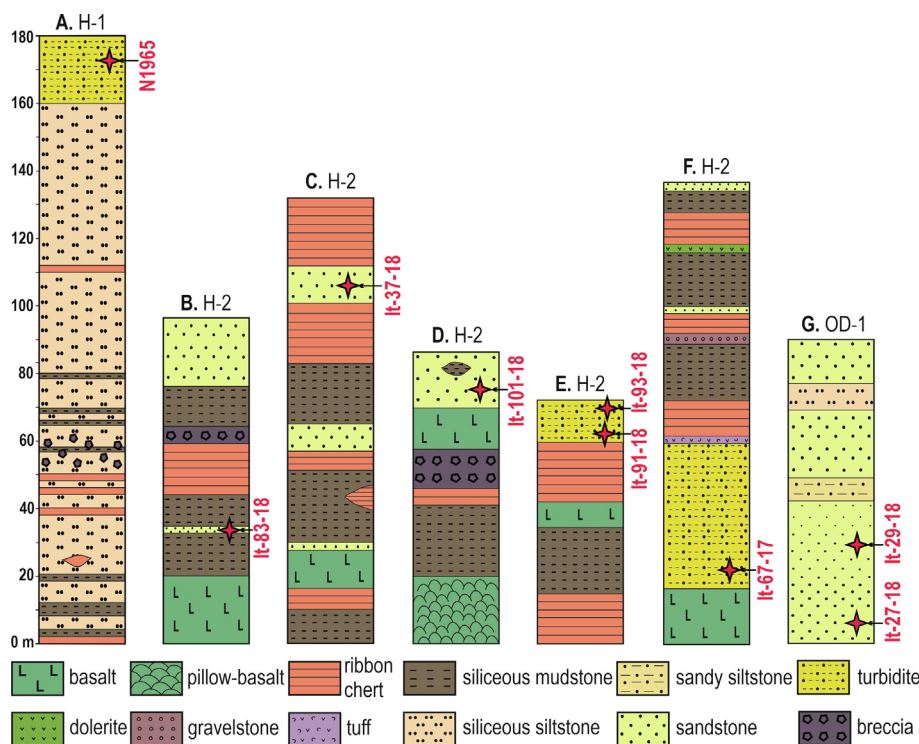


Fig. 4. Lithological columns of igneous and sedimentary rocks of the Itmurundy and Tyuretai fms. outcropped at Sites H-1 (A) and H-2 (B-F) and Site OD-1 (G). Stars are for sandstones samples for U-Pb dating. For the location of sites see Figs. 2 and 3. All columns show separate OPS packages starting from basalt to pelagic ribbon chert, hemipelagic siliceous mudstone and siltstone, and then to more coarse-grained clastic sediments (silty sandstone, sandstone, gravelstone). Most contacts between various lithologies are tectonic or non-identifiable.

(Figs. 6, 7). The fine- to medium-grained, grey and green-grey sandstones of Site H-1 are unsorted and carry poorly rounded to angular lithic fragments and mineral grains 0.1 to 0.3 mm in diameter (Fig. 6A, B). The lithic fragments are aphyric volcanic rocks with plagioclase laths (30–35 %) and siliceous sediments (chert, siliceous mudstone; 30–32 %), and the mineral grains are plagioclase (20–22 %), K-feldspar (7–8 %) and quartz, monocrystalline and polycrystalline (<6 %). The size of the fragments and grains of Site H-2 dark-grey and greenish-grey sandstones is more variable compared to that of Site H-1 sandstones, although most Site H-2 samples are also fine- to medium-grained. The degree of sorting is low and the lithic fragments of various volcanic rocks (35–60 %) and siliceous sediments (14–40 %), the mineral grains of plagioclase (14–20 %), quartz (6–8 %), and K-feldspar (<1 %) are also angular to weakly rounded. The major accessory minerals in the samples from both sites are zircon and epidote. All samples are poorly-cemented sandstones that have matrix consisting of dark fine-grain materials (Fig. 6).

The samples from sites OD-1 and OD-2 are different from those of sites H-1 and H-2 in color, structure and petrography (Fig. 6D-F). The samples of Site OD-1 are light-grey medium- to coarse-grained sandstones, which semi-rounded to rounded poorly sorted clastic grains are quartz (37–44 %), plagioclase (16–22 %), K-feldspar (<2 %) and lithic fragments of igneous rocks (24–38 %) and siliceous sediments (2–4 %) (Fig. 6D) (Supplementary table S1). The major accessory minerals are zircon, muscovite and iron hydroxides. The samples of Site OD-2 are light-greyish-green and coarse-grained (Fig. 6E, F). They carry well-rounded quartz (43–55 %), semi-rounded grains of plagioclase (14–22 %) and K-feldspar (3–5 %), and fragments of igneous (13–15 %) and sedimentary (3–9 %) rocks (Supplementary table S1). The lithic fragments in the sandstones of both sites include chert and siliceous mudstone and mafic to felsic volcanic rocks with porphyritic and hyalopilitic

texture and granites. The matrix is dominated by materials formed by transportation-related brittle deformation and secondary alteration of unstable detrital minerals and lithic fragments. The major accessory minerals are zircon, tourmaline and muscovite.

Compared to Group 1 sandstones (sites H-1 and H-2), Group 2 sandstones (sites OD-1, OD-2) are characterized by higher contents of quartz (up to 55 %) and the presence of fragments of felsic rocks. The presence of mafic to andesitic and andesitic to felsic volcanic rocks as fragments in the sandstones of Group 1 and Group 2, respectively, suggests their volcanomictic character but derivation from compositionally different igneous provenances. All samples experiences secondary chloritization and sausseritization, but to a variable degree.

For further classification and tectonic discrimination, we performed detailed petrographic counting by standard methods (Galehouse, 1971) in twelve thin sections (Supplementary table S1). We counted at least 300 grains of lithic rock and mineral fragments (Lv – volcanic, Ls – sedimentary), quartz (Q) and feldspar (F). According to the classification of Shutov (1967), Group 1 sandstones are greywackes and feldspar greywackes and those of Group 2 are feldspar-quartz greywackes and greywacke arkoses (Fig. 7A). According to the classification of Folk (1980), Group 1 sandstones are litharenite and feldspatic litharenite and those of Group 2 are all feldspatic litharenite (Fig. 7B).

4. Results

4.1. U-Pb detrital zircon dating

The 40 to 200 μm long zircon grains are transparent and yellowish and euhedral to subhedral in shape suggesting relatively short transportation before deposition (proximal source). Cathodoluminescence images (for CL photos see Suppl. Electr. materials)

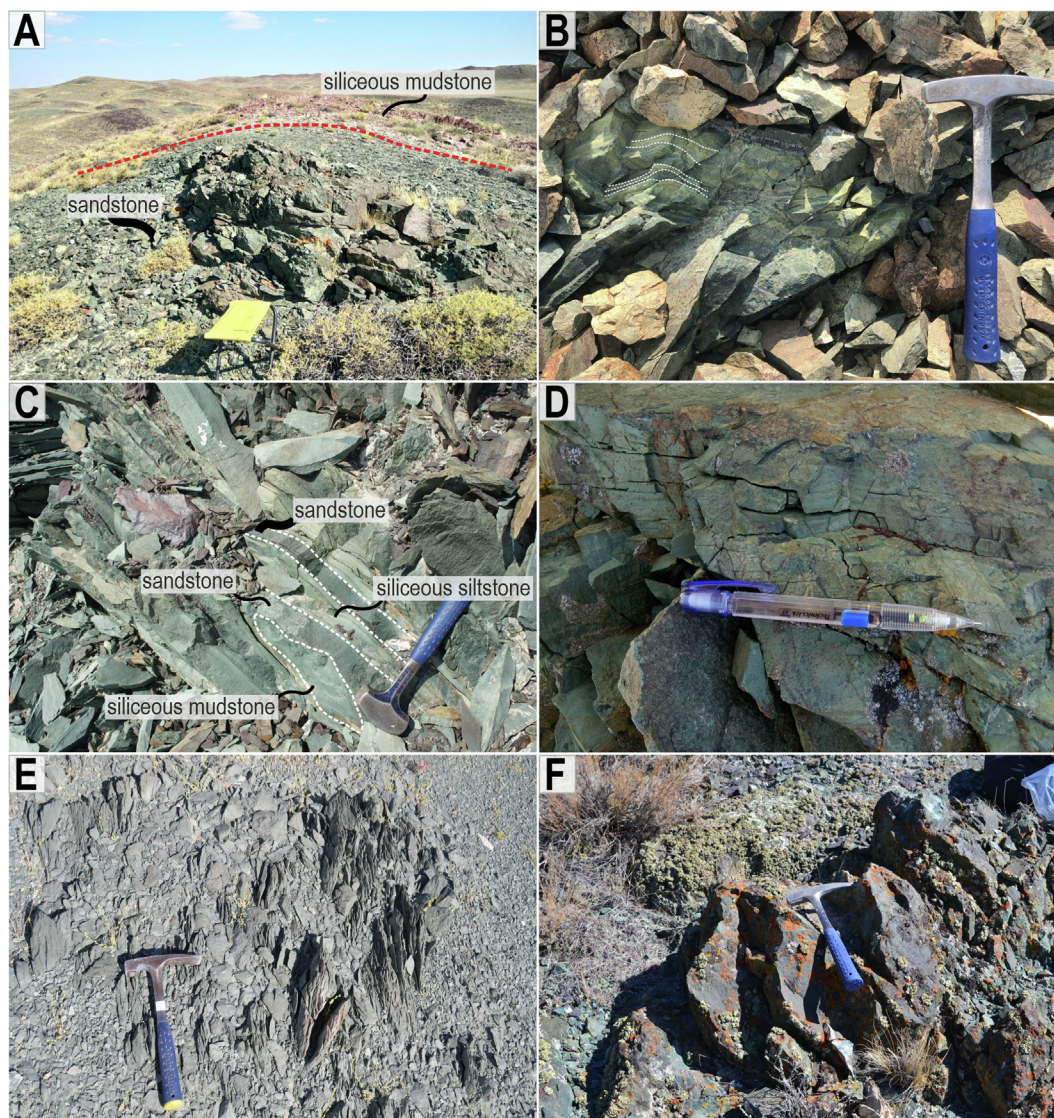


Fig. 5. Photographs of outcrops: a – boundary between sandstones and siliceous mudstones (Site H-1); b – turbidite (Site H-2, sample It-67–17); c – turbidite (Site H-2, sample It-67–17); d – turbidite (Site OD-1, samples It-29–17, It-29–18); e – fine-grained sandstone (Site OD-2); f – medium-grained sandstone (Site OD-2).

show that most of zircons possess oscillatory zoning. Th/U values for all analyzed zircons are higher than 0.13, but lower than 2.25 implying their igneous origin (Hanchar and Hoskin, 2003) (see supplementary Table S2). Typical metamorphic Th/U ratios (<0.1) were found only in 10 grains of a total of 461 grains. For the U-Pb ratios and ages of detrital zircons see supplementary Table S2.

We separated zircons from sandstones of sites H-1, H-2 (Group 1) and OD-1, OD-2 (Group 2). In Site H-1 sandstones (samples It-03–17 and N1965), we analyzed 125 grains, of which 87 grains yielded concordant ages with a concordance higher than 95% (supplementary Table S2). The concordant ages vary from 428 Ma to 536 Ma. The U-Pb age spectrum is generally unimodal with a major peak at ca. 467 Ma (Fig. 8A). The weighted average of the youngest cluster, which was calculated according to (Coutts et al., 2019), is 439.0 ± 6.5 Ma (supplementary figure S2). In the three samples sandstones from Site H-2 (It-67–17, N1956 and It-93–18), we also analyzed 125 grains, of which 98 yielded concordant U-Pb ages (supplementary Table 1S). The U-Pb age spectrum for the three samples is also unimodal with a major peak at ca. 456 Ma (Sandbian); the youngest age is 440 Ma and the oldest is

504 Ma (Fig. 8B). The weighted average of the youngest cluster is 442.0 ± 2.9 Ma (supplementary figure S2).

In the sandstones of Site OD-1 (samples It-29–17 and It-29–18), 120 zircon grains were analyzed, of which 92 grains yielded U-Pb isotope ratios and calculated ages with concordance higher than 95%. The united U-Pb age spectrum of the samples is polymodal with a major peak at 461 Ma (Fig. 8C). The other age populations can be grouped into the intervals of 617–808 Ma ($n = 6$), 895–1169 Ma ($n = 13$) and 2344–2603 ($n = 9$) plus single ages of 1378, 1639, 1720, 1890, 2089 Ma. The weighted average of the youngest cluster is 427.4 ± 4.4 Ma (supplementary figure S2). For Site OD-2 we obtained 91 ages (sample 17081704) including 78 concordant values ranging from 456 Ma to 3406 Ma (Fig. 8D). The distribution of the ages is also polymodal with two major peaks at 462 and 992 Ma. All the data can be grouped into the following intervals: 456–487 Ma ($n = 14$); 824–998 Ma ($n = 19$); 1000–1142 Ma ($n = 9$); 1589–1734 Ma ($n = 5$); 2421–2501 ($n = 13$) plus single values at 2688, 2826, 2929, 3406 Ma. The weighted average of the youngest cluster is 458.8 ± 3.04 Ma (supplementary figure S2).

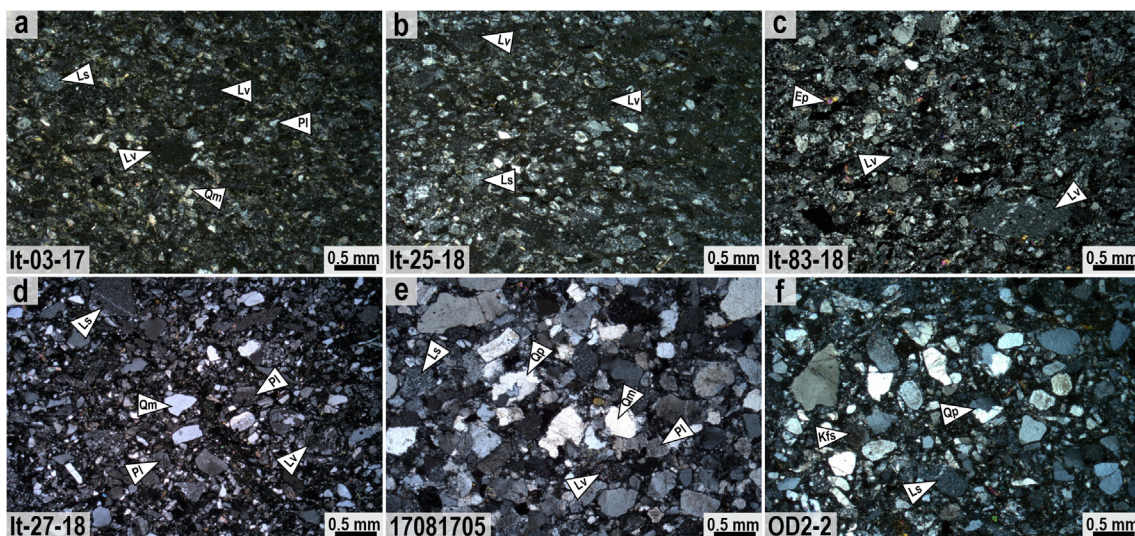


Fig. 6. Photomicrographs of greywacke sandstones of the Itmurydy AC. Abbreviations: Qm = monocrystalline quartz; Qp = polycrystalline quartz; Pl = plagioclase; Kfs = K-feldspar; Ls = sedimentary rock fragments; Lv = volcanic rocks fragments.

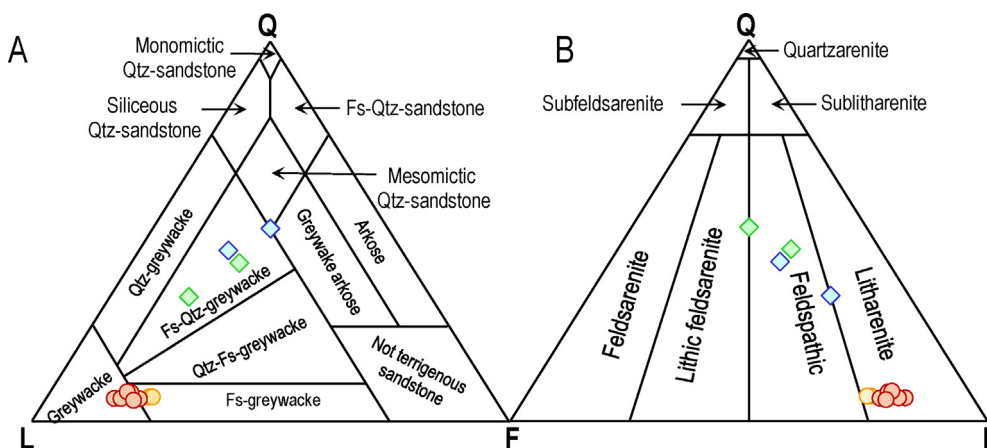


Fig. 7. Petrography counting based classification triangle plots: A, after [Shutov, 1967](#); B, after [Folk, 1980](#). Symbols: circles for Group 1 (yellow and pink for sites H-1 and H-2, respectively), rhombs for Group 2 (green and blue for sites OD-1 and OD-2, respectively).

4.2. Whole-rock geochemistry

Twenty-two whole-rock samples of sandstone were analyzed for major oxides and trace element (supplementary Table S3). The sandstones of all localities show relatively wide variations of SiO₂ contents: 55.2 to 72.6 wt% for sites H-1, H-2 (SiO_{2av.} = 62.7-wt%; N = 16) and 52.6 to 74.6 wt% for sites OD-1, OD-2 (SiO_{2av.} = 65.9 wt%; N = 6). Hereinafter, we consider the sandstones of two groups: Group 1 (sites H-1 and H-2) and Group 2 (OD-1 and OD-2). In comparison with the Post-Archean Australian average shale (PAAS) ([Taylor and McLennan, 1985](#)), these sandstones are depleted in Al₂O₃ and enriched in Fe₂O₃ and MgO, but those of Group 1 possess higher Fe₂O₃ (6.7 wt% in average) compared to Group 2 (5.9 wt% in average) implying a generally more mafic source. In the classification diagram of Pettijohn and co-authors ([Pettijohn et al., 1972](#)), the samples under study plot in the fields of greywacke and litharenite ([Fig. 9](#)), which accords well with their petrographic composition. The high Na₂O/Al₂O₃ ratio of 0.20 to 0.37 most studied samples are also typical of greywackes ([Pettijohn et al., 1972](#)).

Group 1 sandstones show SiO₂ contents spanning the range of 55.2 to 69.7 wt%, which are below or a bit higher than that of the average upper continental crust (UCC; 66.6 wt%) and post-

Archean Australian shales (PAAS; 62.4 wt%) ([Taylor and McLennan, 1985](#)). The content of SiO₂ in Group 2 sandstones ranges from 52.6 to 74.6 wt%, i.e., mostly higher than those of the UCC and PAAS (Supplementary table S3). All these samples are characterized by negative correlations between SiO₂ and TiO₂, Al₂O₃, Fe₂O₃, and MgO implying weak major element fractionation during sedimentation, i.e. the greywackes under study are first cycle sediments ([Fig. 10A-D](#)). In respect to UCC and PAAS, the sandstones are depleted in Al₂O₃ and enriched in MgO ([Fig. 10B, D](#)). The SiO₂/Al₂O₃ ratios of both groups range from 2.89 to 8.50 (4.72 in average) (Supplementary table S3), indicating a low degree of sorting and deposition close to sources because the ratio of SiO₂/Al₂O₃ is indicative of sediment differentiation, weathering and maturity (e.g., [Zhang, 2004](#)).

The Chemical Index of Alteration (CIA) and the Index of Compositional Variability (ICV) characterize weathering features and source composition (mature vs. immature) of sedimentary rocks, respectively ([Nesbitt and Young, 1982](#); [McLennan et al., 1993](#); [Cox and Lowe, 1995](#); [Fedo et al., 1995](#)). The low CIA values for both groups ranging from 44.8 to 65.4 (53.6 in average) suggest a relatively low degree of chemical weathering ([Fig. 11](#)). The CIA values of Group 1 sandstones are in average lower than those of Group 2 (52 vs. 54). This suggests a less weathered source of Group 1 sand-

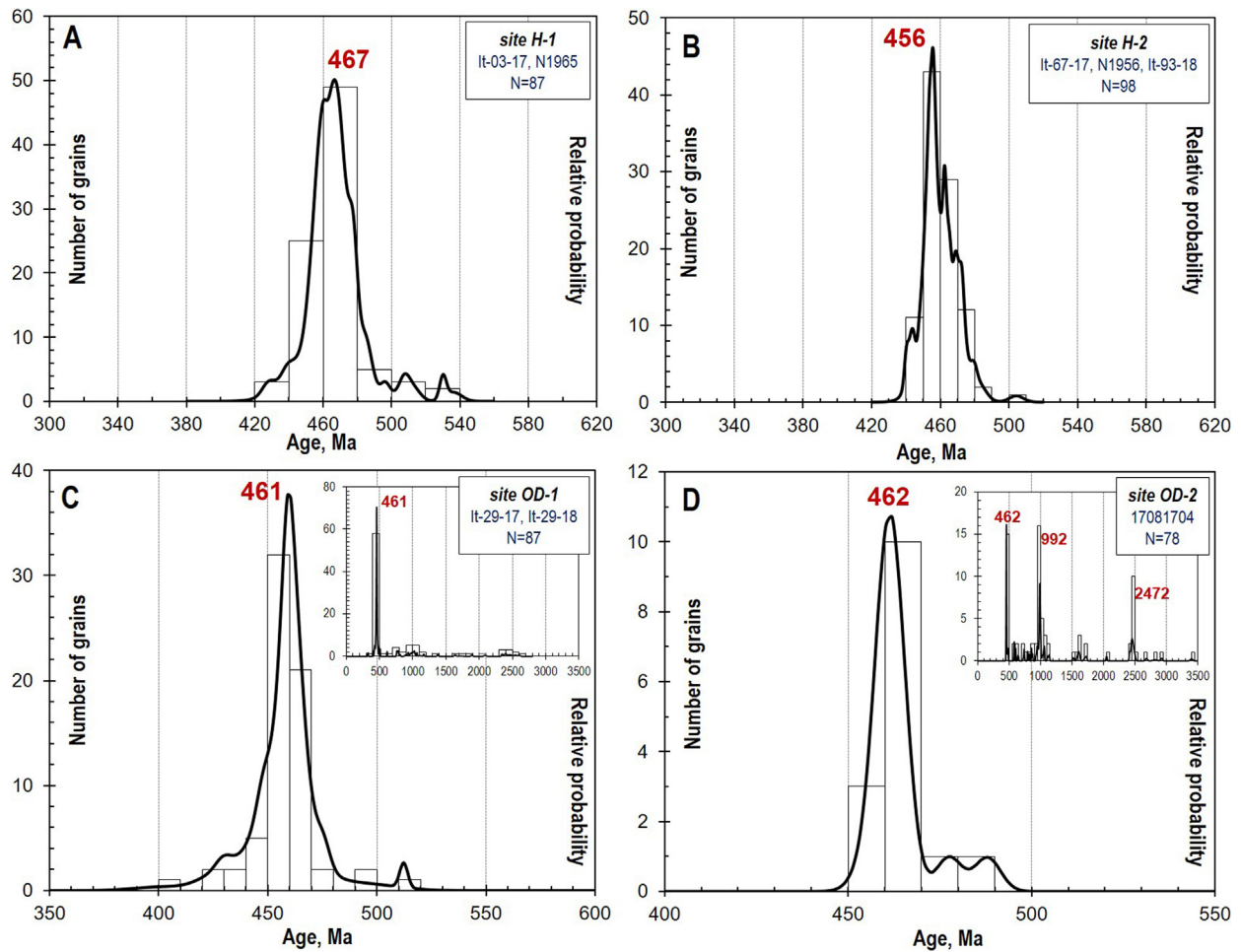


Fig. 8. Histograms and probability curves of the U-Pb ages of detrital zircons from greywacke sandstones of the Itmurundy AC. A, site H-1; B, site H-2; C, site OD-1; D, site OD-2.

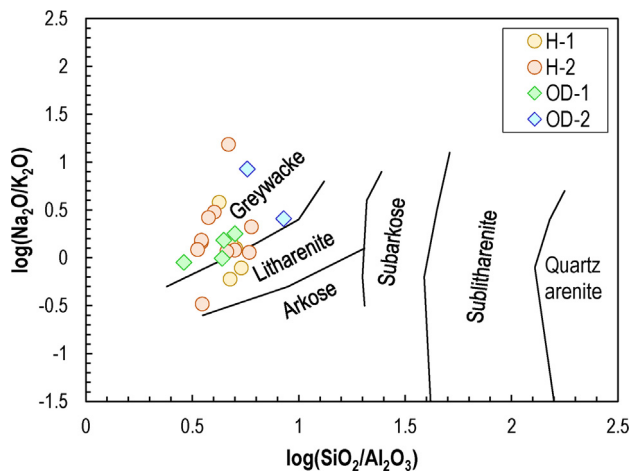


Fig. 9. The $\log(\text{SiO}_2/\text{Al}_2\text{O}_3) - \log(\text{Na}_2\text{O}/\text{K}_2\text{O})$ classification diagrams for greywacke sandstones of the Itmurundy AC after (Pettijohn et al., 1972). Symbols as in Fig. 7.

stones before deposition. All the samples under study are characterized by high ICV values ranging from 1.3 to 2.5 (1.8 in average) suggesting an immature source dominated by non-clay silicate minerals.

In terms of trace elements, Group 1 samples have slightly higher Sr than those of Group 2 (supplementary Table S3) implying

more plagioclase in the source rocks (Feng and Kerrich, 1990). Scandium for all sandstones is positively correlated with the content of Fe suggesting a relatively mafic igneous source. Compared to PAAS, the greywackes under study show lower concentrations of REE and other incompatible elements (Fig. 12A, B). The concentrations of K_2O are positively correlated with those of Rb, negatively with Sr and neutrally with Ba (Supplementary figure S3). The REE patterns of both groups show enrichment in the LREE ($\text{La}/\text{Yb}_n = 2.2\text{--}9.8$) and zero to weakly differentiated HREE ($\text{Sm}/\text{Yb}_n = 1.3\text{--}3.0$) (Fig. 12A). Group 1 samples show less fractionated LREE compared to Group 2 ($\text{La}/\text{Yb}_{n,\text{av.}} = 4.2$ vs 9.3 and $\text{La}/\text{Sm}_{n,\text{av.}} = 2.2$ vs 3.6). All REE spectra show similar moderate negative Eu anomalies ($\text{Eu}/\text{Eu}^*_{\text{av.}} = 0.76$), similar to that of PAAS ($\text{Eu}/\text{Eu}^* = 0.65$; Taylor and McLennan, 1985), that is a characteristic feature of magmatic rocks undergone fractional crystallization of plagioclase, like many supra-subduction compositionally intermediate lavas. The primitive mantle normalized multi-element spectra for all samples show clear Nb negative anomalies relative to La ($\text{Nb}/\text{La}_{\text{pm}} = 0.2\text{--}1.0$) and Th ($\text{Nb}/\text{Th}_{\text{pm}} = 0.1\text{--}0.8$) (Supplementary table S3; Fig. 12B, D) and accordingly resemble those of supra-subduction/arc volcanic rocks (e.g., Pearce, 1982; Briquieu et al., 1984).

4.3. Whole-rock Nd and Hf-in-zircon isotopes

Whole-rock Nd isotopic composition of sediments is a key to understand the nature of their igneous protoliths. In this paper,

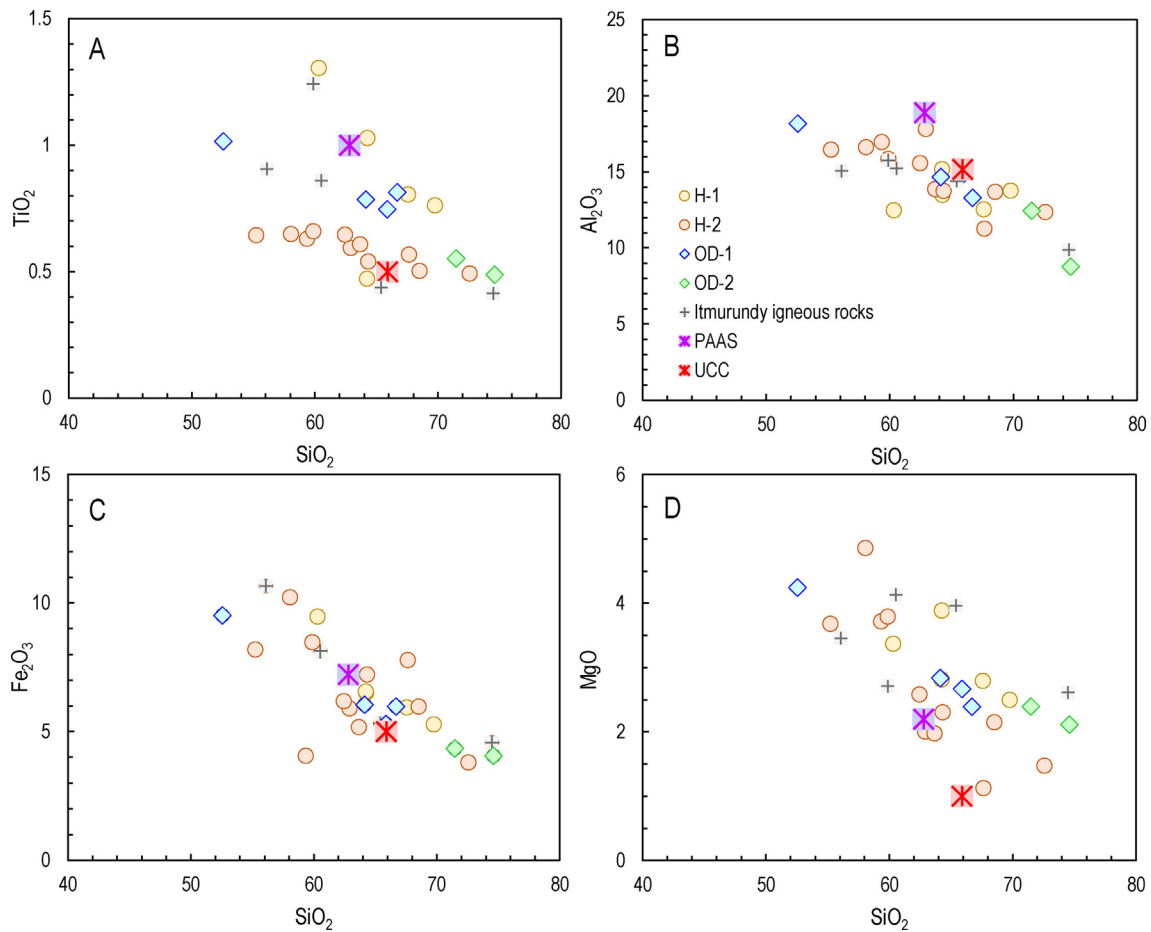


Fig. 10. SiO₂ vs major oxides for greywacke sandstones and igneous rocks of the Itmurundy AC. The compositions of Itmurundy volcanic rocks are from (Safonova et al., 2020).

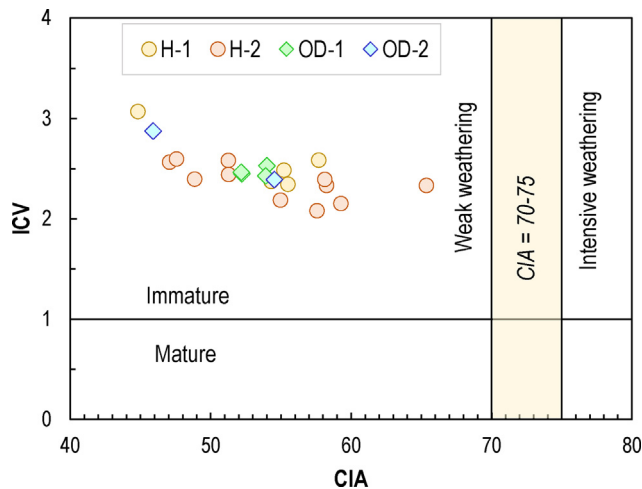


Fig. 11. CIA-ICV diagram for greywacke sandstones of the Itmurundy AC. The yellow area is for the range of CIA values of Post-Archean Australian Shale, PAAS (Taylor and McLennan, 1985). The index of chemical alteration, CIA = $[Al_2O_3 / (Al_2O_3 + CaO^* + Na_2O + K_2O)] \times 100$, where CaO* is the content of CaO in silicate minerals only, is given after (Nesbitt and Young, 1982) and the Index of Compositional Variability, ICV = $(CaO + K_2O + Na_2O + Fe_2O_3 + MgO + MnO + TiO_2) / Al_2O_3$ is given after (Cox and Lowe, 1995).

we present first Sm-Nd isotopic data from three samples of the greywacke sandstones (Supplementary table S4). The measurements of Sm-Nd isotope ratios were made in the Geological

Institute of the Kola Science Center, Apatity, Russia (for details on methodology see Suppl. Electr. materials). For isotope measurements we selected the freshest samples with lowest LOI. The isotope evolution diagram (Fig. 13A) shows the Nd isotope ratios and calculated indicative values. The initial isotopic ratios were calculated using microfossil and depositional ages (Safonova et al., 2019; Supplementary table S2; Fig. 8).

Group 1 samples (It-09-18, It-75-18, H1-7/1, It-91-18) are characterized by positive $\epsilon Nd(t)$ values (+1, +5.3, +4.0, +6.6) with Nd model ages of $T_{DM} = 1.5$ to 0.7 Ga (Fig. 13A; Supplementary table S4). The samples have $^{147}Sm/^{144}Nd$ ratios between 0.1509 and 0.1422; the measured ratios of $^{143}Nd/^{144}Nd$ are from 0.512548 to 0.512820, respectively. Their related values of T_{DM2} are from 1.1 to 0.67 Ga. On the contrary, Group 2 sample (It-29-18, OD2-2, 17081704) yielded negative $\epsilon Nd(t)$ values of -7.5 to 3.9 with the Nd model ages (T_{DM}) of 1.96 to 1.6 Ga. The samples have $^{147}Sm/^{144}Nd = 0.1300, 0.1250$ and 0.1244 , $^{143}Nd/^{144}Nd = 0.512073, 0.512220$ and 0.512034 , and $T_{DM2} = 1.8, 1.5$ and 1.8 Ga, respectively (Fig. 13A; supplementary Table S4).

We analyzed Hf isotopes in zircons from all four sites (Fig. 13B; supplementary Table S5). The zircons from sandstones of Group 1 yielded strongly positive $\epsilon Hf(t)$ values. Ten zircons from sample It-03-17 (site H-1) and seven zircons from sample It-67-17 (site H-2) of Group 1 yielded $\epsilon Hf(t)$ values ranging from + 9.2 to + 16 and from + 13.3 to + 17.5, respectively. The values of $\epsilon Hf(t)$ recorded in Group 2 sandstones are much more variable. In Group 2, twenty zircons from sample It-29-17 (site OD-1), seven zircons from sample It-29-18 (site OD-1) and 21 zircons from sample 17,081,704 (site OD-2) yielded wide ranges of $\epsilon Hf(t)$ from -24.5 to + 10.56 (T^{ϵ}

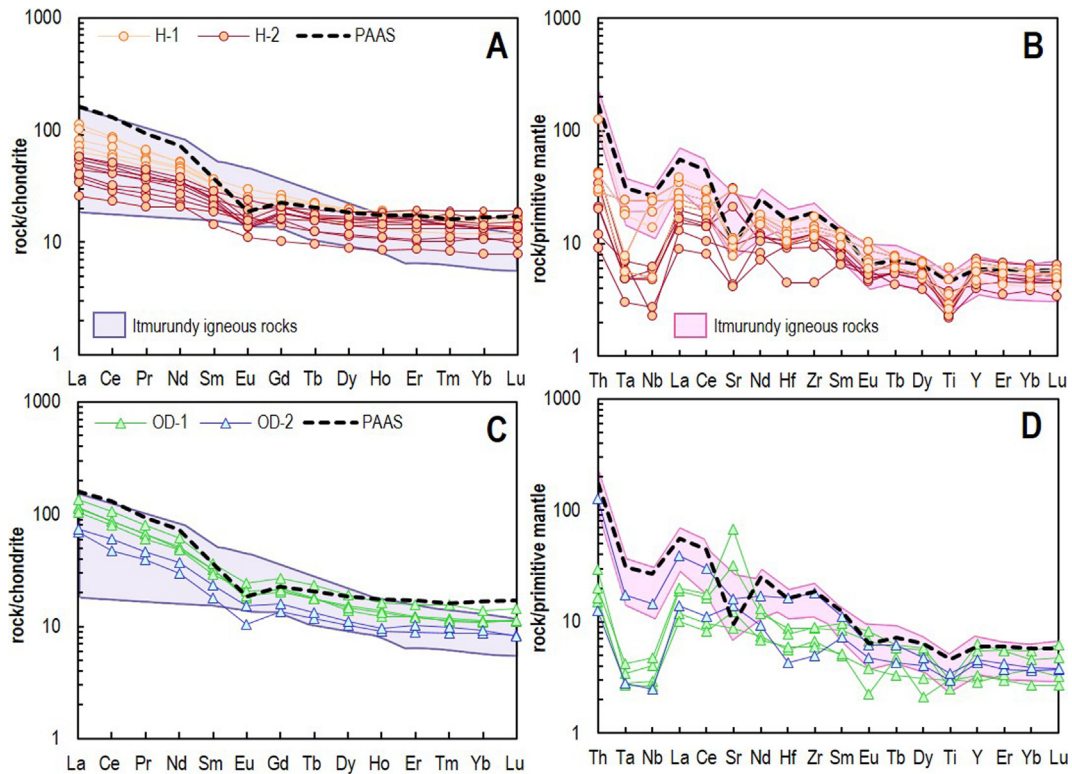


Fig. 12. Chondrite-normalized REE patterns (A, C) and primitive mantle multi-element diagrams (B, D) for greywacke sandstones of the Itmurundy AC. The normalizing values of chondrite and primitive mantle are from Sun and McDonough (1989) and that of PAAS is from Taylor and McLennan (1985).

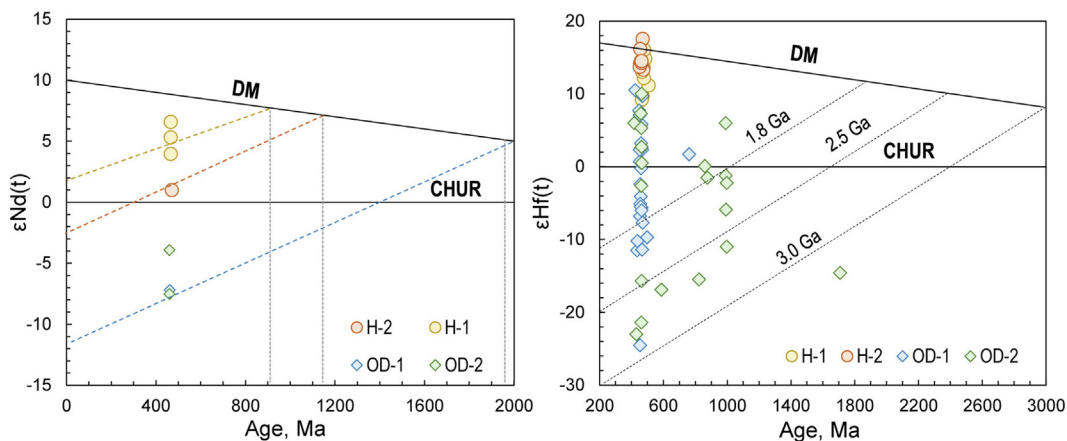


Fig. 13. Whole rock Nd and Hf-in-zircon isotope data from greywacke sandstones of the Itmurundy ACs. A, the age (in Ma) versus $\epsilon_{Nd}(t)$ diagram. B, the age (in Ma) versus $\epsilon_{Hf}(t)$ diagram; the values of $\epsilon_{Nd}(t)$ and $\epsilon_{Hf}(t)$ were calculated based on the microfauna-based depositional ages and U-Pb zircon ages (sections 1 and 4.1; Supplementary table S2).

$T_{Hf}^{DM} = 2541\text{--}688$ Ma), from -11.4 to $+7.7$ ($T_{Hf}^{DM} = 1874\text{--}856$ Ma) and from -23 to $+10$ ($T_{Hf}^{DM} = 3055\text{--}746$ Ma), respectively. Thus, the zircons from sandstones of sites H-1, H-2 (Group 1) show only positive $\epsilon_{Hf}(t)$ values, whereas zircons from sandstones of sites OD-1, OD-2 (Group 2) are characterized by $\epsilon_{Hf}(t)$ varying from strongly negative to strongly positive values.

5. Discussion

5.1. Itmurundy greywacke sandstones and ocean plate stratigraphy

There are various clastic sediments including greywacke sandstones in the study area. The Early Paleozoic volcanogenic-

siliceous units of the Itmurundy zone and have been studied since the 1980-ies, mostly for stratigraphy and paleontology though (e.g., Patalakha and Belyi, 1981; Novikova et al., 1983; Zhyilkaidarov, 1998). The possible provenances, depositional environments, and igneous protoliths have remained unclear. In theory, sandstones may belong to the accretionary complex, i.e. formed in trench as a part of turbidite association, or to the supra-subduction complex, i.e. formed in a fore-arc and/or back-arc basin. Our previous studies have shown that the supra-subduction igneous rocks occur together with the igneous (MORB, OIB; Safonova et al., 2020; Perfilova et al., 2022) and sedimentary rocks of the accretionary complex (Fig. 2). Direct contacts of igneous and sedimentary rocks are rare. Most contacts between

different accreted lithologies are tectonic (Figs. 2–4). The accreted packages are typically folded, thrust under and over each other (Safonova et al., 2019, 2020). Such an extremely complicated structure is typical of all accretionary complexes worldwide (e.g., Wakita, 2012; Kusky et al., 2013; Safonova, 2017). The tectonic juxtaposition of Itmurundy accretionary and supra-subduction complexes makes hard to differentiate the Itmurundy sandstones of different origins, based only on geological information.

According to the geological map (Fig. 2), the sandstones under study belong to the Itmurundy Fm., sites H-1 and H-2 (Group 1), and to the Tyuretai Fm., sites OD-1 and OD-2 (Group 2), exposed, respectively, in the central and eastern segments of the Itmurundy AC (Figs. 2, 3). The lithological columns (Fig. 4) show (bottom to top) mafic volcanic rocks (basaltic lavas), pelagic ribbon chert, hemipelagic sediments (siliceous mudstone and siltstone), and terrigenous rocks (greywacke/turbidite sandstones, gravelstone). The overall succession of volcanic and sedimentary rocks perfectly fits the ocean plate stratigraphy (e.g., Isozaki et al., 1990; Maruyama et al., 2010; Kusky et al., 2013; Safonova et al., 2016). The sandstones of both groups are associated with siliceous mudstone and siltstone to form turbidites (Figs. 4, 5). The turbidite accumulated in trench is also part of OPS and typically occurs in the upper part of PS succession of package/. All sections under study show turbidite sandstones in the upper part of each OPS package and contain two and more sandstone layers suggesting OPS duplexing (Fig. 4). However, the different geological, geochemical and isotopic characteristics of the sandstones of two groups record different provenances.

5.2. Source provenance and igneous protoliths

In general, the petrographic features and geochemical compositions of the Itmurundy sandstones suggest their derivation through destruction of volcanic rocks of the Itmurundy zone (Safonova et al., 2020; Perfilova et al., 2022). The sandstones of both sites carry clasts of aphyric and porphyric volcanic rocks (Fig. 6). However, cement-free Group 1 sandstones have low contents of quartz, high contents of feldspar and abundant clasts of mafic to andesitic volcanic rocks and siliceous sediments suggesting their greywacke character (Fig. 7A; supplementary Table 1S). The sandstones of Group 2 are characterized by higher contents of quartz, presence of andesitic to felsic volcanic rocks as clasts and fine-grained cement. Their petrography indicate they are quartz-bearing to arkose greywackes, i.e., probably derived from more acidic magmatic complexes.

In general, the major element compositions of both clastic and volcanic rocks of the Itmurundy zone are close to andesite (Fig. 10; Safonova et al., 2020; Perfilova et al., 2022). More specifically, clastic sediments deposited in different tectonic settings have been studied by many researchers (e.g., Bhatia and Taylor, 1981; Bhatia and Crook, 1986; Roser and Korsch, 1986; McLennan et al., 1993; McLennan and Taylor, 1991). Sandstones derived from intra-oceanic island arcs typically have higher Al_2O_3 , $Fe_2O_3 + MgO$, TiO_2 , and lower SiO_2 , SiO_2/Al_2O_3 , Na_2O/K_2O compared to those derived from continental arcs. Group 1 sandstones have higher values of Al_2O_3 (av. 14.5 wt%) and a sum of $Fe_2O_3 + MgO$ (av. 9.5 wt%) compared to Group 2 sandstones ($Al_2O_3 = 14.5$, $\Sigma Fe_2O_3 + MgO = 9.5$ wt% in average). More evidence for the derivation of greywackes from supra-subduction igneous rocks come from the similar REE and multi-element patterns obtained from both igneous and clastic rocks of the Itmurundy AC (Fig. 12).

The trace element composition of clastic sediments also can be used to determine provenance type (e.g., Bhatia and Crook, 1986; McLennan et al., 1993) based on the enrichment of mafic rocks in HFSE (e.g. Zr, Nb, Ta, Y) and REE compared to felsic rocks. In addition,

basaltic melts are characterized by higher Sc and Co resulting in higher Co/Th and lower La/Sc ratios (McLennan et al., 1993). The Itmurundy sandstones of Group 1 yielded higher Co/Th (2.5–18.5) and lower La/Sc (0.4–1.5), Zr/Sc (2.36–11.72) and Th/Sc (0.05–0.27) ratios compared to Group 2 samples (1.02–2.04 and 1.27–1.84, 6.32–15.82, 0.39–0.91, respectively) (Fig. 14A–C). The compositions of the sandstones under study clearly follow a trend from mafic to felsic sources (Fig. 14A) suggesting a change of provenance from that dominated by basalt and andesibasalt to that dominated by andesitic to dacitic igneous rocks. In general, all trace-element data suggest that the greywacke sandstones of Group 1 (central segment of the Itmurundy zone; Figs. 2, 3A) were derived from a source dominated by basaltic and/or andesitic igneous rocks, while the sandstones of Group 2 from that by andesitic to dacitic igneous rocks (eastern segment of the Itmurundy zone; Figs. 2, 3B). In addition, the Nd whole-rock and Hf-in-zircon data (Fig. 13) indicate that Group 1 greywacke sandstones formed by destruction of igneous rocks derived from juvenile magma sources, but the provenance of Group 2 sandstones included rocks derived from both juvenile and recycled sources or from sources with mixed isotope characteristics.

5.3. Deposition rate and maximum depositional age

The petrographic features of the sandstones under study (Figs. 6, 7; supplementary Table S1) show abundant lithic fragments and feldspars, which are commonly less stable during distant transportation and long burial. In terms of whole-rock geochemistry, the values of SiO_2/Al_2O_3 and Na_2O/K_2O classifying them as litharenites and greywackes (Fig. 9) and the high ICV and low CIA values (Fig. 11) are all suggestive of their compositional immaturity (Pettijohn et al., 1972). The strong inter-element correlations, which are well seen in the geochemical diagrams (Fig. 14), also suggest that studied greywackes are first cycle sediments. The greywacke sandstones of both localities show relatively wide variations of Zr/Sc at a narrower range of Th/Sc, which are positively correlated in the Zr/Sc–Th/Sc diagram (Fig. 14B). These characteristics also suggest that the provenance of the greywackes was controlled rather by source composition than by sediment recycling (McLennan et al., 1993; Cullers, 1994). Thus, all petrographic and geochemical characteristics coupled with the textural and compositional immaturity of the Itmurundy sandstone indicate that (1) they were probably deposited close to the sediment sources, i.e. experienced short-distant transportation, poor sorting and rapid burial, and (2) that their provenance was dominated by weakly weathered igneous rocks.

Of special importance is the timing of sedimentation of Group 1 and Group 2 sandstones, which could be inferred from microfossil and U–Pb age zircon data, but until recently has remained debatable. The sandstones of Group 1 (the central segment; Figs. 2, 3A) are associated with OPS units of the Itmurundy Fm., which early-middle Ordovician age was constrained by conodonts from pelagic ribbon chert and hemipelagic siliceous mudstone (Novikova et al., 1983; Safonova et al., 2019; Degtyarev et al., 2020a). This microfossil-based age range agrees well with the ca. 480–440 Ma major peak of the U–Pb ages of detrital zircon from Group 1 sandstones (Fig. 8A, B). These age constraints indicate that deep-marine sedimentation in the ocean was coeval with the Ordovician supra-subduction magmatism at its active margin. However, the maximum depositional ages of Group 1 sandstones constrained by the youngest cluster of U–Pb zircon ages, are 442 and 439 Ma suggest that the main stage of clastic sedimentation was during the Llandovery (Fig. 8A, B; supplementary Fig. S2).

The sandstones of Group 2 (the eastern segment; Figs. 2, 3B) are a dominant lithology of the Tyuretai Fm., which late Ordovician – early Silurian age was defined by conodonts from chert and grap-

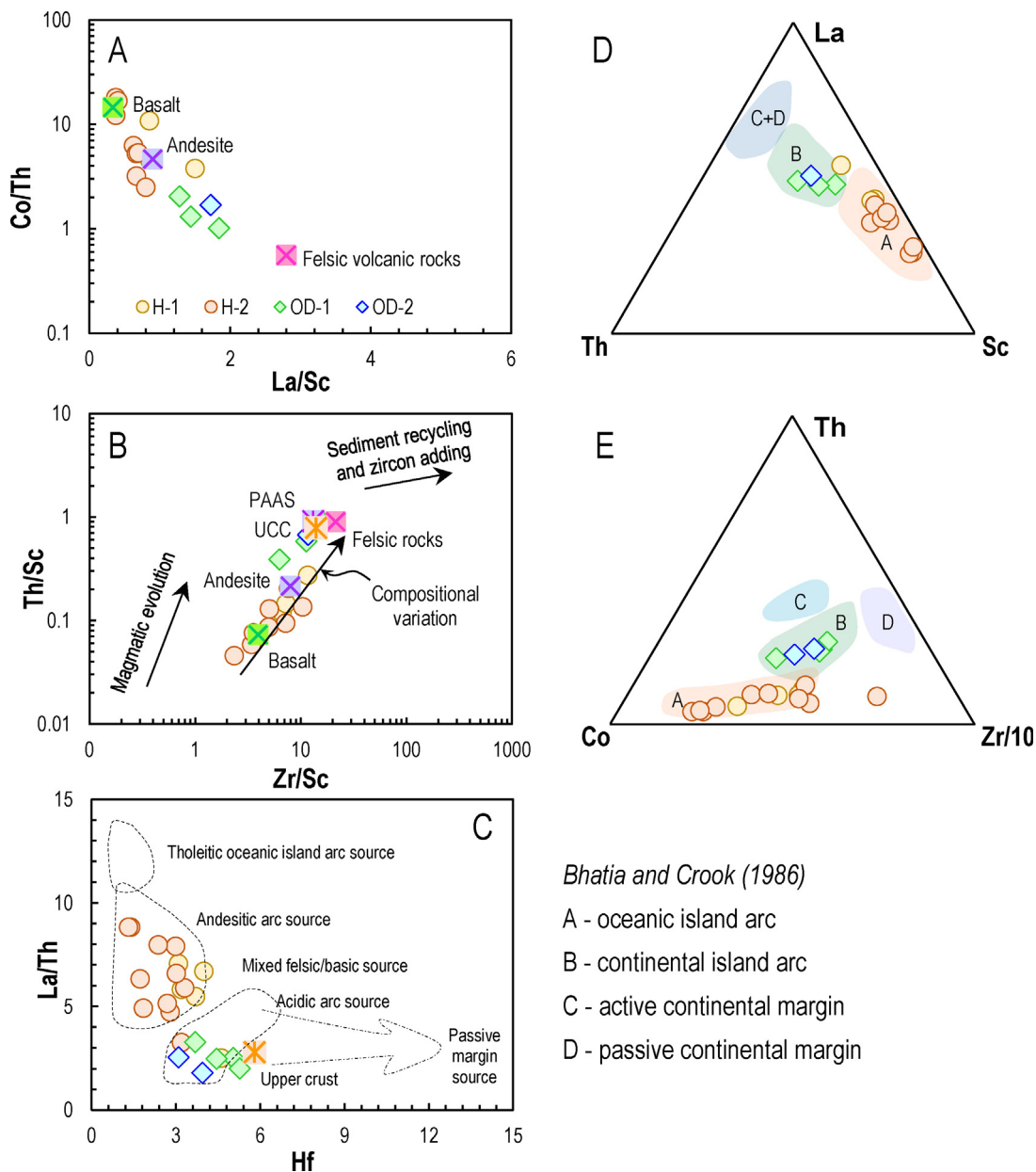


Fig. 14. Discrimination diagrams for greywacke sandstones of the Itmurundy AC: (a) La/Sc vs. Co/Th and (b) Zr/Sc vs. Th/Sc (after McLennan et al., 1993); (c) Hf vs. La/Th (after Floyd and Leveridge, 1987); (d) Th-La-Sc, (t) Co-Th-Zr/10 (Bhatia and Crook, 1986).

tolites from silty sandstone (Novikova et al., 1983; Zhylkaidarov, 1998). These age constrains partly overlap with the ca. 475–445 Ma major peak of Group 2 U-Pb ages (Fig. 8C, D). However, the Group 2 sandstones yielded two different maximum depositional ages from sites OD-1 and OD-2: 427 and 459 Ma, respectively, i.e. the main stage of sedimentation of OD-1 sandstones was during the Ludlow, i.e. a bit later than that recorded in Group 1 sandstones (Fig. 8; supplementary figure S2).

5.4. Tectonic implications

The abundant poorly sorted angular lithic fragments (Fig. 6) and the immature geochemical features (Fig. 11) of the Itmurundy greywacke sandstones suggest their derivation from a closely located magmatic complex/protolith and rapid burial. All four spectra of the U-Pb ages of detrital zircon from all samples show major peaks at ca. 467–456 Ma suggesting derivation from a single

arc (Fig. 8). However, only the sandstones of Group those from 1 (sites H-1 and H-2) are unimodal. Those from the sandstones of Group 2 are polymodal, i.e. show Precambrian ages. In general, unimodal distributions of U-Pb detrital zircon ages are typical of intra-oceanic arcs built on a young mafic basement, e.g. the Mariana arc and Alaska arcs (Barth et al., 2017; Schmitt et al., 2018; Box et al., 2019). The petrographic (greywacke vs litharenite), geochemical (mafic vs felsic) and isotope (juvenile vs recycled) characteristics of the sandstones allows us to suggest their formation through destruction of an intra-oceanic and/or continental arc.

The protolithic complex of Group 1 sandstones was probably dominated by mafic to andesitic volcanic rocks (Fig. 14A-C). In the Th-La-Sc and Co-Th-Zr/10 ternary plots, the compositional points of Group 1 plot in the fields of oceanic island arc (Fig. 14D, E). In the F-L-Q petrography-based discrimination triangle diagrams of Dickinson and co-authors (Dickinson et al., 1983) Group 1 sandstones plot in the field of undissected arc, i.e., a young

intra-oceanic arc (Fig. 15). The stepped line in the left side of Fig. 15 shows increasing amount of lithic fragments, volcanic rocks in our case, and feldspars from Group 1 to Group 2 also suggesting different provenances or a change of magmatism in the source area from dominantly andesibasaltic to andesidacitic, respectively. Such a trend may happen if a volcanic arc evolved from primitive to mature that is typical of long-living arcs, e.g., the Mariana and other intra-oceanic arcs (e.g., Ishizuka et al., 2011; Ribeiro et al., 2020).

The U-Pb detrital zircon age spectra of Group 1 sandstones are clearly unimodal with major peaks at 467 and 456 Ma (Fig. 8A, B). The positive values of whole-rock $\epsilon Nd_{(t)}$ and zircon $\epsilon Hf_{(t)}$ are indicative of igneous rocks melted from a juvenile mantle source (Fig. 13). The volcanic rocks with juvenile source characteristics are more typical of intra-oceanic arcs, e.g., Mariana and Bonin (e.g., Lin et al., 1990; Pearce et al., 1999; Woodhead et al., 2012). In addition, the central part of the Itmurundy zone, i.e. the locus of Group 1 sandstones, hosts andesibasalts, andesites and boninite-like basalts also typical of intra-oceanic arcs (Safonova et al., 2017; Safonova et al., 2020). All features suggest the derivation of Group 1 sandstones from a late Ordovician intra-oceanic and their accumulation in a fore-arc setting/trench, at a Mariana-type convergent margin of the Paleo-Asian Ocean (Fig. 16).

The protolithic igneous complex of Group 2 sandstones is obviously dominated by andesitic to dacitic volcanic rocks (Fig. 14-A-C). In the Th-La-Sc and Co-Th-Zr/10 ternary plots (Fig. 14D, E), the compositional points of Group 2 plot in the field of continental arc. In the F-L-Q triangle diagrams (Fig. 15), Group 2 sandstones plot in the field of recycled orogen and in the fields of transitional and dissected arc (Site OD-1) and mixed arc (Site OD-2). The U-Pb detrital zircon age spectra of Group 2 sandstones are also generally unimodal with major peaks at 461 and 460 Ma, but show minor (Fig. 8C) to moderate (Fig. 8D) amounts of Precambrian ages ranging from 2.5 Ga to 750 Ma. The values of whole-rock $\epsilon Nd_{(t)}$ and zircon $\epsilon Hf_{(t)}$ are negative and negative-to-positive, assuming recycled and mixed mantle sources, respectively (Fig. 13). Negative $\epsilon Nd_{(t)}$ values are more typical of continental arcs sitting on old and/or compositionally mixed basement (e.g., Wörner et al., 1992;

Barrágan et al., 1998). Therefore, Group 2 sandstones were also derived from a late Ordovician intra-oceanic, but accumulated in a late Ordovician to early Silurian back-arc basin, which provenances were fed by material coming from both, continental arc and intra-oceanic arc (Fig. 16). The much smaller amount of Precambrian zircons in the sandstones of Site OD-1 suggests that they deposited closer to the intra-oceanic arc compared to the sandstones of Site OD-2, i.e. the OD-2 sandstones accumulated closer to the continental arc. That continental arc probably existed at an Andean-type convergent margin of the Paleo-Asian Ocean. The oldest zircons, which number is very small though could be derived from microcontinents of the West Junggar-Yili region (Wang et al., 2022), e.g., the Aktau-Junggar microcontinent.

Thus, the U-Pb ages from all sandstones showing peaks within the interval of 475 to 445 Ma coupled with geochemical and isotope data indicate a long period of intra-oceanic arc magmatism during almost the whole Ordovician. The youngest U-Pb zircon ages range from 440 to 428 Ma suggesting that the attenuation of magmatism and related active sedimentation started in early Silurian. There are very few ages in the range of 490–480 Ma but about 20 ages in the range of 512–480 Ma (Supplementary Table S2; Fig. 8). These middle-late Cambrian ages accord well with the U-Pb ages of plagiogranites present as serpentine-hosted blocks of the East Arkharsu (520 Ma) and Kentaralau (498–476 Ma) ultramafic–mafic massifs (Fig. 2) (Degtyarev et al., 2021a). In addition, the Kentaralau serpentinite mélange includes blocks of ca. 502 Ma supra-subduction diorite (Safonova et al., 2020). Thus, there were two stages of supra-subduction magmatism. The first started in the late Cambrian, because arc diorite and plagiogranite from serpentinite mélange in the central segment of the Itmurundy zone yielded, respectively, the U-Pb zircon ages of 502 ± 4 (Safonova et al., 2020) and 498 ± 8 Ma (Degtyarev et al., 2021a) (Fig. 2). The second stage formed the Ordovician arc recorded in the sandstones of the Itmurundy accretionary complex (480–440; Fig. 8A, B). In general, the presence of igneous arc-related rocks in serpentinite mélange is suggestive of subduction erosion (Suzuki et al., 2010; Maruyama and Safonova, 2019). In the Itmurundy zone, the presence of supra-subduction 520–

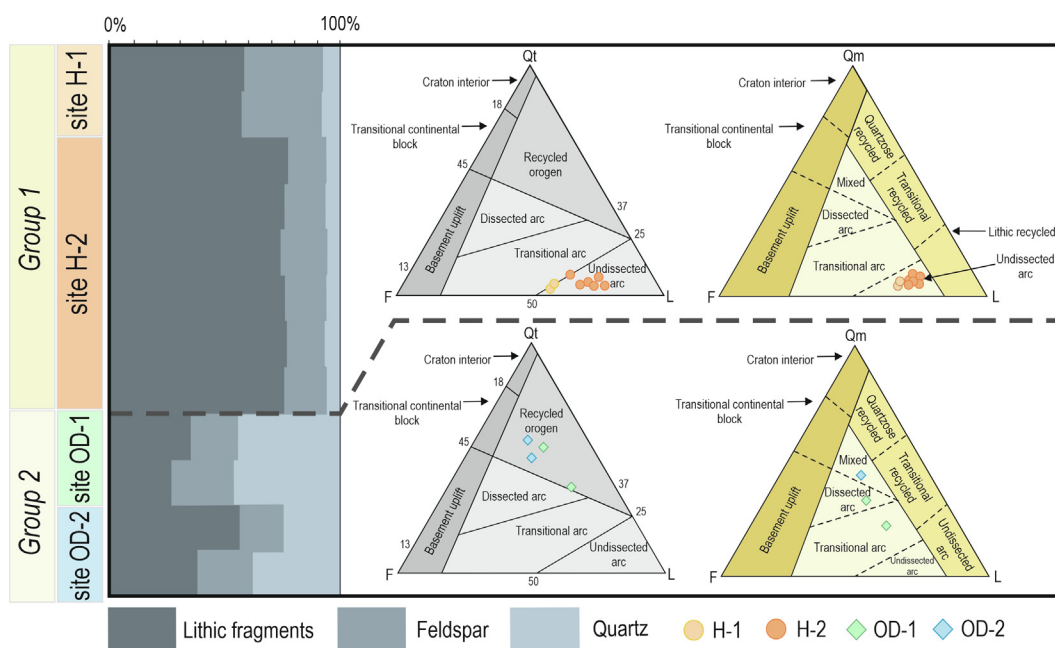


Fig. 15. A summary of petrographic counting of greywacke sandstones of the Itmurundy AC. The ternary plots (Dickinson et al., 1985) show geodynamic settings of potential provenances. Qm – monocrystalline quartz, Qt – total quartz, F – feldspar, L – total lithic fragments.

498 Ma plagiogranites and diorites as blocks in serpentinite mélangé, the limited amount of 512–480 Ma ages of detrital zircons with juvenile Hf and Nd isotope features (Supplementary table S5) and the scarcity and/or small size of outcrops of igneous rocks with supra-subduction geochemical characteristics (Figs. 2, 3) all allow us to suggest that there was also a middle-late Cambrian intra-oceanic arc, which later was tectonically eroded (e.g., Scholl and von Huene, 2007; Stern, 2010; Safonova, 2017).

5.5. Geodynamic model

There have been identified many intra-oceanic arc complexes in Kazakhstan indicating a continuous subduction from Cambrian to at least Devonian time in the adjacent areas of Kazakhstan and farther to the south-east, i.e. in the NW China (Fig. 1) (Safonova et al., 2017 and references therein). However, few fragments of Middle to late Cambrian intra-oceanic arcs have been identified in the study region and around, except for those of Late Cambrian age only found in limited amounts within the Boschekul-Chingiz or Chingiz-Tarbagatai arc (Degtyarev, 2011; Shen et al., 2015). The middle to late Cambrian and early Ordovician supra-subduction granitoids found in the Itmurundy zone (Safonova et al., 2020; Degtyarev et al., 2021a) occur only as fragments/blocks in the Kentaralau and East Arkharsu serpentinite mélanges (Fig. 2). On the contrary, in addition to the Itmurundy zone (Safonova et al., 2020; Degtyarev et al., 2021a), there are a lot of occurrences of Ordovician volcanic rocks in other regions of central Kazakhstan, e.g., in the Tekturmas and Chingiz-Boshchekul zones (Khasse

et al., 2020; Degtyarev et al., 2021b), southern Kazakhstan (Alexeiev et al., 2011), West Junggar (e.g., Xu et al., 2013; Zheng et al., 2019). Our new data from greywacke sandstones coupled with the recent data from igneous rocks (Safonova et al., 2020; Degtyarev et al., 2021b) allow us to propose a model for the evolution of the Itmurundy zone (Fig. 16).

In middle to late Cambrian time, a magmatic arc existed at an active margin of the western Paleo-Asian Ocean probably near the Aktau-Junggar microcontinent (Figs. 1, 16A). Later, that arc was tectonically eroded and its pieces (granitoids) detached from the hanging wall of the subduction zone got incorporated into the serpentinite mélangé formed along the subduction channel (Fig. 16B, C). The subduction erosion was responsible for the fast subsidence of the active margin, the cessation of magmatism and the shift of the trench axis toward the microcontinent. In early Ordovician time, an intra-oceanic arc was initiated (Fig. 16B). The surface erosion of the arc supplied clastic material to both fore-arc and back-arc basins. The deposits of the fore-arc basin including the trench contained only the clastic material of the Ordovician intra-oceanic arc and consequently the distributions of the U-Pb ages of their hosted detrital zircons are all unimodal (Fig. 8A, B). There are two types of back arc basin deposits: those carrying very few Precambrian zircons – Site OD-1 sandstones (Fig. 8C) and those carrying about 20% of those – Site OD-2 sandstones (Fig. 8D). The Site OD-1 sandstones deposited later, during the Ludlow, probably much closer to the arc and much farther from the (micro)continent compared to the OD-2 sandstone (Fig. 16C). The latter deposited earlier, during the Sandbian, prob-

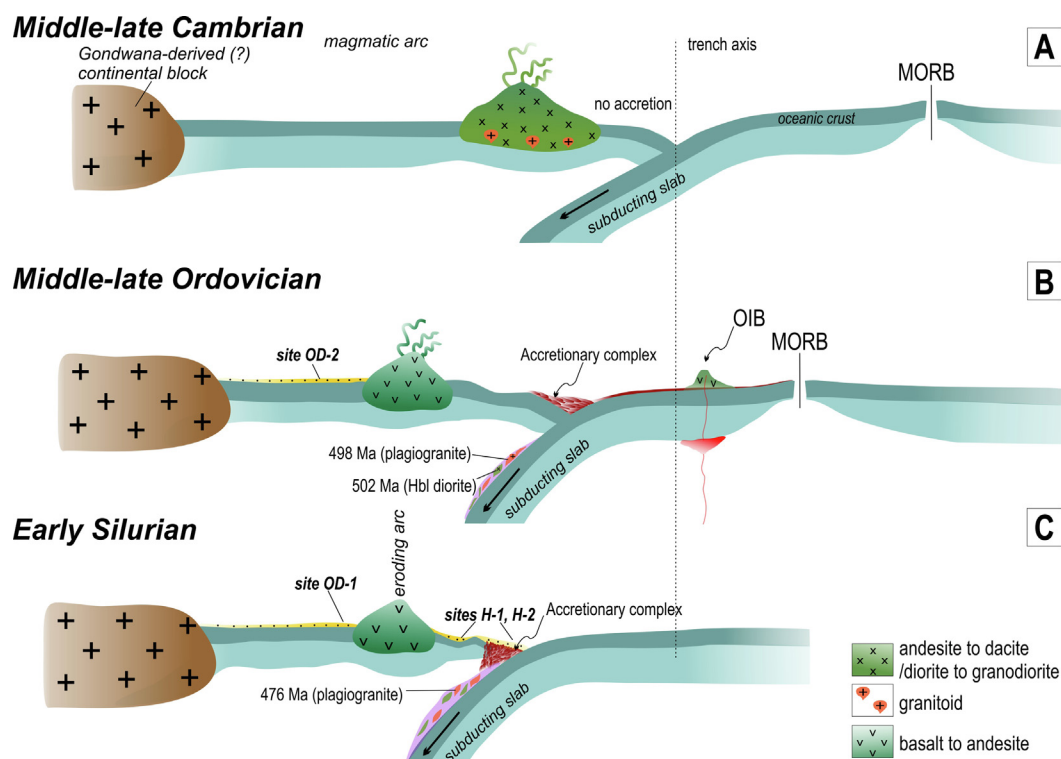


Fig. 16. A geodynamic model showing two stages of intra-oceanic arc magmatism (A, B) and different settings of clastic sedimentation in respect to the greywacke sandstones of Group 1 and Group 2 of the Itmurundy AC (C). A, the middle-late Cambrian magmatic arc dominated by granitoids was destroyed by subduction erosion. B, the middle-late Ordovician mafic-andesitic intra-oceanic arc served a source for the greywacke sandstones of the Itmurundy AC; simultaneously an accretionary complex grew oceanward to incorporate the pieces of oceanic crust peeled off the subducting plate. The sedimentation of OD-2 (Group 2) sandstones started in Sandbian time relatively close to the (micro)continental block. C, the volcanism ceased and the active sedimentation of H-1 and H-1 sandstones (Group 1) started in Llandoveryan time in a fore-arc basin and trench. The deposition of OD-1 samples (Group 2) started in Ludlow time and proceeded in a back-arc basin, closer to the remnant intra-oceanic arc (Group 2a)). Pieces of diorite and plagiogranite were captured by the serpentinite mélangé, which was squeezed up to the surface along the subduction channel. A Gondwana-derived continental block could be the Aktau-Junggar microcontinent serving a source of Precambrian zircon to Group 2 sandstones (Fig. 1; Windley et al., 2007). All geological elements are shown out of scale. The U-Pb zircon ages from igneous rocks (Fig. 16B) are from (Safonova et al., 2020; Degtyarev et al., 2020b, 2021a).

ably much farther from the arc, but closer to the (micro)continent (Fig. 16B). We think that in post-Sandbian time, the provenance of the OD-2 sandstone was isolated from younger zircon-bearing volcanogenic material.

The intra-oceanic arc magmatism fully ceased by the late Silurian. The intensive deposition of the Group 1 sandstones started at ca. 441–439 Ma (Llandovery). The exhumation of serpentinite mélange could take place after 476 Ma, the youngest age of plagiogranite in mélange (Fig. 16C), but before the Ludlow because the serpentinite mélanges are bounded by faults ending at those separating the orogenic formations from the post-orogenic ones (Fig. 2).

6. Conclusions

The Itmurundy AC hosts the full succession of ocean plate stratigraphy (OPS): basalt, pelagic chert, hemipelagic siliceous mudstone and siltstone, and sandstones. The sandstones under study crop out in the central (Group 1) and eastern (Group 2) segments of the Itmurundy zone. The sandstones of both segments occur in the upper parts of sedimentary sections that is typical of OPS. The petrographic and geochemical features of all sandstones are indicative of their greywacke composition and immature and weakly weathered character, i.e., they are first cycle sediments deposited close to the source are of their igneous protoliths.

All four spectra of the U-Pb ages of detrital zircon from all samples show major peaks at ca. 467–456 Ma. The distributions of the U-Pb ages of zircons from Group 1 sandstones are unimodal suggesting their derivation from in an intra-oceanic arc and deposition in a fore-arc basin and deep trench. The greywackes of Group 2 contain minor to medium amounts of Precambrian zircons suggesting their accumulation in a back-arc basins but closer to the arc and closer to the microcontinent. The youngest ages of all sandstones are ca. 436–424 Ma indicate the start of active sedimentation in early Silurian time and the intra-oceanic arc magmatism fully ceased during the late Silurian.

Geochemically, the sandstones are similar to the Itmurundy volcanic rocks of supra-subduction origin. The different geochemical and isotopic characteristics of the two groups of sandstones record different provenances: mafic-andesitic and andesidacitic. The Hf-in-zircon and whole-rock Nd data suggest that Group 1 greywacke sandstones formed by destruction of igneous rocks derived from juvenile magma sources, but the provenance of Group 2 sandstones included rocks derived from both juvenile and recycled sources. The limited amount of 512–480 Ma ages of detrital zircons with juvenile Hf and Nd isotope features in all zircon spectra, the occurrence of supra-subduction igneous rocks only as blocks in serpentinite mélange suggest tectonic erosion of a Cambrian intra-oceanic arc.

Records of two magmatic arcs have been found in the Itmurundy zone: (1) the middle-late Cambrian magmatic arc, that was tectonically eroded and its pieced preserved only in serpentinite mélange, and (2) the middle-late Ordovician intra-oceanic arc, which served a source of the greywacke sandstones of the Itmurundy accretionary complex.

CRedit authorship contribution statement

Inna Safonova: Conceptualization, Writing – review & editing, Project administration, Funding acquisition. **Alina Perfilova:** Investigation, Writing – original draft. **Ilya Savinskiy:** . **Pavel Kotler:** Software. **Min Sun:** Methodology, Data curation. **Bo Wang:** Methodology, Data curation.

Declaration of Competing Interest

The authors declare that they have no known competing financial interests or personal relationships that could have appeared to influence the work reported in this paper.

Acknowledgements

We would like to express our cordial thanks to Prof. Santosh for editorial handling and to Dr. T. Ota and two anonymous reviewers for their constructive and useful comments and suggestions, which all helped us to improve the manuscript to a significant extent. Many thanks to the staff of the analytic centers in Novosibirsk and Yekaterinburg (CUC “Geoanalyst”). The study was supported by the Russian Science Foundation, Project # 21-77-20022 (geochronology, stratigraphy, petrography, geochemistry, geodynamic implications, paper preparation). We also acknowledge the Ministry of Science and Education of Russia, Projects #0330-2019-0003 (regional geology), AAAA-A19-119072990020-6 (Nd isotopes), FSUS-2020-0039 (tectonics), the Ministry of Science and Education of Kazakhstan (project #AP08855920; local geology), the Hong Kong Research Grants Council (HKU17302317, U-Pb isotopes), the National Nature Science Foundation of China (projects # 41772225, 42161144013, Hf isotopes). Contribution to IGCP#662.

Appendix A. Supplementary data

Supplementary data to this article can be found online at <https://doi.org/10.1016/j.gr.2022.06.018>.

References

- Alexeev, D.V., Ryazantsev, A.V., Kröner, A., Tretyakov, A.A., Xia, X., Liu, D.Y., 2011. Geochemical data and zircon ages for rocks in a high-pressure belt of Chu-Yili Mountains, southern Kazakhstan: Implications for the earliest stages of accretion in Kazakhstan and the Tianshan. *J. Asian Earth Sci.* 42 (5), 805–820.
- Barrágan, R., Geist, D., Hall, M.L., Larson, P., Kurz, M., 1998. Subduction controls on the composition of lavas from the Ecuadorian Andes. *Earth Planet. Sci. Lett.* 154, 153–166.
- Barth, A.P., Tani, K., Meffre, S., Wooden, J.L., Coble, M.A., Arculus, R.J., Ishizuka, O., Shukle, J.T., 2017. Generation of silicic melts in the early Izu-Bonin arc recorded by detrital zircons in proximal arc volcanoclastic rocks from the Philippine Sea. *Geochem. Geophys. Geosyst.* 18 (10), 3576–3591.
- Bhatia, M.R., Crook, K.A.W., 1986. Trace element characteristics of greywackes and tectonic setting discrimination of sedimentary basins. *Contrib. Mineral. Petrol.* 92, 181–193.
- Bhatia, M.R., Taylor, S.R., 1981. Trace element geochemistry and sedimentary provinces: a study from the Tasman Geosyncline. *Australia. Chem. Geol.* 33 (1–4), 115–125.
- Box, S.E., Karl, S.M., Jones III, J.V., Bradley, D.C., Haeussler, P.J., O’Sullivan, P.B., 2019. Detrital zircon geochronology along a structural transect across the Kahiltina assemblage in the western Alaska Range: Implications for emplacement of the Alexander-Wrangellia-Peninsular terrane against North America. *Geosphere* 15, 1774–1808.
- Briqueu, L., Bougault, H., Joron, J.L., 1984. Quantification of Nb, Ta, Ti and V anomalies in magmas associated with subduction zones: petrogenetic implications. *Earth Planet. Sci. Lett.* 68 (2), 297–308.
- Buslov, M.M., Saphonova, I.Y., Watanabe, T., Obut, O.T., Fujiwara, Y., Iwata, K., Semakov, N.N., Sugai, Y., Smirnova, L.V., Kazansky, A.Y., 2001. Evolution of the Paleo-Asian Ocean (Altai-Sayan region, Central Asia) and collision of possible Gondwana-derived terranes with the southern marginal part of the Siberian continent. *J. Geosci.* 5 (3), 203–224.
- Clift, P.D., Vannucchi, P., 2004. Controls on tectonic accretion versus erosion in subduction zones: implications for the origin and recycling of the continental crust. *Rev. Geophys.* 42, RG2001.
- Coutts, D.S., Matthews, W.A., Hubbard, S.M., 2019. Assessment of widely used methods to derive depositional ages from detrital zircon populations. *Geoscience Frontiers* 10 (4), 1421–1435.
- Cox, R., Lowe, D.R., 1995. A conceptual review of regional-scale controls on the composition of clastic sediment and the co-evolution of continental blocks and their sedimentary cover. *J. Sediment. Res.* 1, 1–12.
- Cullers, R.L., 1994. The Controls on the Major and Trace Element Variation of Shales, Siltstones, and Sandstones of Pennsylvanian-Permian Age from Uplifted Continental Blocks in Colorado to Platform Sediment in Kansas, USA. *Geochim. Cosmochim. Acta* 58 (22), 4955–4972.

- Degtyarev, K.E., 2011. Tectonic evolution of early Paleozoic island arc systems and continental crust formation in the Caledonides of Kazakhstan and the North Tien Shan. *Geotectonics* 45 (1), 23–50.
- Degtyarev, K.E., Luchitskaya, M.V., Tretyakov, A.A., Pilitsyna, A.V., Yakubchuk, A.S., 2021a. Early Paleozoic suprasubduction complexes of the North Balkhash ophiolite zone (Central Kazakhstan): Geochronology, geochemistry and implications for tectonic evolution of the Junggar-Balkhash Ocean. *Lithos* 380–381, 105818.
- Degtyarev, K.E., Tolmacheva, T.Y., Tretyakov, A.A., 2020a. Siliceous–volcanic associations of the Northern Balkhash ophiolite Zone (Central Kazakhstan): Biostratigraphy, sedimentation and tectonic evolution in the Middle–Late Ordovician. *Palaeogeogr., Palaeoclimat., Palaeoecol.* 551, 109748.
- Degtyarev, K.E., Yakubchuk, A.S., Luchitskaya, M.V., Tretyakov, A.A., 2020b. Age and structure of a fragment of the Early Cambrian ophiolite sequence (North Balkhash Zone, Central Kazakhstan). *Doklady Earth Sci.* 491 (1), 111–116.
- Degtyarev, K., Yakubchuk, A.S., Luchitskaya, M.V., Tolmacheva, T.Yu., Skoblenko (Pilitsyna), A.V., Tretyakov, A.A., 2021b. Ordovician supra-subduction, oceanic and within-plate ocean island complexes in the Tekturmas ophiolite zone (Central Kazakhstan): age, geochemistry and tectonic implications. *Int. Geol. Rev.* <https://doi.org/10.1080/00206814.2021.1969691>.
- Dickinson, W.R., Beard, L.S., Brakenridge, G.R., Erjavek, J.L., Ferguson, R.C., Inman, K. F., Knepp, R.A., Lindberg, F.A., Ryberg, P.T., 1983. Provenance of North American Phanerozoic Sandstones in Relation to Tectonic Setting. *Geol. Soc. Am. Bull.* 94 (2), 222–235.
- Dickinson, W.R., Szczech, C.A., 1979. Plate Tectonics Sandstone Compositions. *Am. Ass. Petrol. Geol. Bull.* 63, 2164–2182.
- Fedo, C.M., Nesbitt, H.W., Young, G.M., 1995. Unraveling the effects of potassium metasomatism in sedimentary rocks and paleosols, with implications for paleoweathering conditions and provenance. *Geology* 23, 921–924.
- Feng, R., Kerrich, R., 1990. Geochemistry of Fine Grained Clastic Sediments in the Archaean Abitibi Greenstone Belt, Canada: Implications for Provenance and Tectonic Setting. *Geochim. Cosmochim. Acta* 54, 1061–1081.
- Folk, R.L., 1980. Petrology of Sedimentary Rocks. Hemphill, Austin. 184 p.
- Galehouse, J.S., 1971. Sedimentation analysis. In: Carver, R. (Ed.), *Procedures in Sedimentary Petrology*. Wiley–Interscience, London, pp. 69–94.
- Hanchar, J.M., Hoskin, P.W.O., 2003. Zircon. *Rev. Mineral. Geochem.* 53, 500 p.
- Ishizuka, O., Tani, K., Reagan, M.K., Kanayama, K., Umino, S., Harijane, Y., Sakamoto, I., Miyajima, Y., Yuasa, M., Dunkley, D.J., 2011. The timescales of subduction initiation and subsequent evolution of an oceanic island arc. *Earth Planet. Sci. Lett.* 306 (3–4), 229–240.
- Isozaki, Y., Maruyama, S., Furuoka, F., 1990. Accreted oceanic materials in Japan. *Tectonophysics* 181 (1–4), 179–205.
- Floyd, P.A., Leveridge, B.E., 1987. Tectonic Environment of the Devonian Gramscatho Basin South Cornwall: Framework Mode and Geochemical Evidence from Turbiditic Sandstones. *J. Geol. Soc. London* 144 (4), 531–542.
- Jahn, B.-M., 2004. The Central Asian Orogenic Belt and growth of the continental crust in the Phanerozoic. *Geological Society, London, Special Publications* 226 (1), 73–100.
- Khanchuk, A.I., Nikitina, A.P., Panchenko, I.V., Burii, G.I., Kemkin, I.V., 1989. Paleozoic and Mesozoic guyots of Sikhote-Alin and Sakhalin. *Doklady AN SSSR* 307 (1), 186–190. In Russian.
- Khassen, B.P., Safonova, I.Y., Yeremolov, P.V., Antonyuk, R.M., Gurova, A.V., Obut, O.T., Perfilova, A.A., Savinskiy, I.A., Tsujimori, T., 2020. The Tekturmas ophiolite belt of central Kazakhstan: Geology, magmatism, and tectonics. *Geol. J.* 55 (3), 2363–2382.
- Konopelko, D., Safonova, I., Perfilova, A., Biske, Y., Mirkamalov, R., Divaev, F., Kotler, P., Obut, O., Wang, B., Sun, M., Soloshenko, N., 2021. Detrital zircon U–Pb–Hf isotopes and whole-rock geochemistry of Ediacaran–Silurian clastic sediments of the Uzbek Tianshan: sources and tectonic implications. *Int. Geol. Rev.* <https://doi.org/10.1080/00206814.2021.2010134>.
- Koshkin, V.Y., Galitsky, V.V., 1960. Geological map of the USSR 1: 200 000. Series Balkhash. Sheet L-43–XI. South Kazakhstan Geological Department of the Ministry of Geology and Mineral Protection of the USSR. [in Russian].
- Kroner, A., Kovach, V., Alexeiev, D., Wang, K.-L., Wong, J., Degtyarev, K., Kozakov, I., 2017. No excessive crustal growth in the Central Asian Orogenic Belt: Further evidence from field relationships and isotopic data. *Gondwana Res.* 50, 135–166.
- Kröner, A., Kovach, V., Belousova, E., Hegner, E., Armstrong, R., Dolgoplova, A., Seltmann, R., Alexeiev, D.V., Hofmann, J.E., Wong, J., Sun, M., Cai, K., Wang, T., Tong, Y., Wilde, S.A., Degtyarev, K.E., Ryttsk, E., 2014. Reassessment of continental growth during the accretionary history of the Central Asian Orogenic Belt. *Gondwana Res.* 25, 103–125.
- Kröner, A., Windley, B., Badarch, G., Tomurtogoo, O., Hegner, E., Jahn, B.M., Gruschka, S., Khain, E.V., Demoux, A., Wingate, M.T.D., 2007. Accretionary growth and crust formation in the Central Asian orogenic belt and comparison with the Arabian–Nubian shield. In: Hatcher, R.D., Jr., Carlson, M.P., McBride, J.H., Martinez Catalan, J.R. (Eds.), *Framework of continental crust*. *Geol. Soc. Am. Mem.* 200, 181–209.
- Kuskuy, T., Windley, B., Safonova, I., Wakita, K., Wakabayashi, J., Polat, A., Santosh, M., 2013. Recognition of Ocean Plate Stratigraphy in accretionary orogens through Earth history: A record of 3.8 billion years of sea floor spreading, subduction, and accretion. *Gondwana Res.* 24, 501–547.
- Lin, Q.H., Li, L.Y., Liang, M.G., 1990. Origin of granitic rocks in the Heshui–Sihe area, western Guangdong. *Reg. Geol. China*, 173–180. In Chinese with English abstract.
- Long, X.P., Yuan, C., Sun, M., Xiao, W.J., Zhao, G.C., Wang, Y.J., Cai, K.D., Xia, X.P., Xie, L.W., 2010. Detrital zircon ages and Hf isotopes of the early Paleozoic flysch sequence in the Chinese Altai, NW China: new constraints on depositional age, provenance and tectonic evolution. *Tectonophysics* 180, 213–231.
- Long, X., Yuan, C., Sun, M., Safonova, I., Xiao, W., Wang, Y., 2012. Geochemistry and U–Pb detrital zircon dating of Paleozoic graywackes in East Junggar, NW China: Insights into subduction–accretion processes in the southern Central Asian Orogenic Belt. *Gondwana Res.* 21, 637–653.
- Maruyama, S., 1997. Pacific-type orogeny revisited: Miyashiro-type orogeny proposed. *Island Arc* 6, 91–120.
- Maruyama, S., Kawai, T., Windley, B.F., 2010. Ocean plate stratigraphy and its imbrication in an accretionary orogen: the Mona Complex, Anglesey–Lleyn, Wales, UK. In: Kusky, T.M., Zhai, M.-G., Xiao, W. (Eds.), *The Evolving Continents: Understanding Processes of Continental Growth*. *Geol. Soc. London, Spec. Pub.* 338, 55–75.
- Maruyama, S., Safonova, I., 2019. Orogeny and Mantle Dynamics: Role of Tectonic Erosion and Second Continent in the Mantle Transition Zone. *Novosibirsk State Univ., Novosibirsk*.
- Matsuda, T., Isozaki, Y., 1991. Well-documented travel history of Mesozoic pelagic chert in Japan: remote ocean to subduction zone. *Tectonics* 10, 475–499.
- McLennan, S.M., Hemming, S., McDaniel, D.K., Hanson, G.N., 1993. Geochemical approaches to sedimentation, provenance and tectonics. In: Johnson, M.J., Basu, A. (Eds.), *Processes controlling the composition of clastic sediments*. *Geol. Soc. Am. Spec. Pap.* 284, 21–40.
- McLennan, S.M., Taylor, S.R., 1991. Sedimentary-Rocks and Crustal Evolution: Tectonic Setting and Secular Trends. *J. Geol.* 99, 1–21.
- Nesbitt, H.W., Young, G.M., 1982. Early Proterozoic climates and plate motions inferred from major element chemistry of lites. *Nature* 299, 715–717.
- Nikitin, I.F., 2002. Ordovician siliceous and siliceous–basalt complexes of Kazakhstan. *Rus. Geol. Geophys.* 43, 512–527.
- Novikova, M.Z., Gerasimova, N.A., Dubinina, S.V., 1983. Conodonts from the volcanic–siliceous complex of the Northern Balkhash. *Doklady AN SSSR* 271, 1449–1451. In Russian.
- Patalakha, F.A., Belyi, V.A., 1981. Ophiolites of the Itmurundy–Kazyk zone. In: Abdulin, A.A., Patalakha, F.A. (Eds.), *Ophiolites of Kazakhstan*. *Nauka, Alma-Ata*, pp. 7–102. In Russian.
- Pearce, J.A., 1982. Trace element characteristics of lavas from destructive plate boundaries, in Thorpe, R.S., ed., *Andesites* 525–548.
- Pearce, T.J., Besly, B.M., Wray, D.S., Wright, D.K., 1999. Chemostratigraphy: a method to improve inter-well correlation in barren sequences – a case study using onshore Devonian/Stephanian sequences (West Midlands, U.K.). *Sediment. Geol.* 124, 197–220.
- Perfilova, A.A., Safonova, I.Y., Gurova, A.V., Kotler, P.D., Savinskiy, I.A., 2022. Tectonic settings of formation of volcanic and sedimentary rocks of the Itmurundy zone, central Kazakhstan. *Geodyn. & Tectonophysics* 13 (1), 0572.
- Pettijohn, F.J., Potter, P.E., Siever, R., 1972. *Sand and sandstone*. Springer, Berlin Heidelberg New York.
- Ribeiro, J.M., Ishizuka, O., Lee, C.-T.-A., Girard, G., 2020. Evolution and maturation of the nascent Mariana arc. *Earth Planet. Sci. Lett.* 530, 115912.
- Roser, B.P., Korsch, R.J., 1986. Determination of tectonic setting of sandstone–mudstone suites using SiO₂ content and K₂O/Na₂O ratio. *J. Geol.* 94, 635–650.
- Safonova, I.Y., 2009. Intraplate magmatism and oceanic plate stratigraphy of the Paleo-Asian and Paleo-Pacific Oceans from 600 to 140 Ma. *Ore Geol. Rev.* 35, 137–154.
- Safonova, I.Y., 2017. Juvenile versus recycled crust in the Central Asian Orogenic Belt: Implications from ocean plate stratigraphy, blueschist belts and intra-oceanic arcs. *Gondwana Res.* 47, 6–27.
- Safonova, I., Komiya, T., L. Romer, R., Simonov, V., Seltmann, R., Rudnev, S., Yamamoto, S., Sun, M., 2018. Supra-subduction igneous formations of the Char ophiolite belt, East Kazakhstan. *Gondwana Res.* 59, 159–179.
- Safonova, I., Kotlyarov, A., Krivonogov, S., Xiao, W., 2017. Intra-oceanic arcs of the Paleo-Asian Ocean. *Gondwana Res.* 50, 167–194.
- Safonova, I., Maruyama, S., Kojima, S., Komiya, T., Krivonogov, S., Koshida, K., 2016. Recognizing OIB and MORB in accretionary complexes: A new approach based on ocean plate stratigraphy, petrology and geochemistry. *Gondwana Res.* 33, 92–114.
- Safonova, I.Y., Perfilova, A.A., Obut, O.T., Savinsky, I.A., Cherny, R.I., Petrenko, N.A., Gurova, A.V., Kotler, P.D., Khromykh, S.V., Krivonogov, S.K., Maruyama, S., 2019. Itmurundy accretionary complex (Northern Balkhash): geological structure, stratigraphy and tectonic origin. *Rus. J. Pac. Geol.* 38, 102–117.
- Safonova, I., Perfilova, A., Obut, O., Kotler, P., Aoki, S., Komiya, T., Wang, B., Sun, M., 2021. Traces of intra-oceanic arcs recorded in sandstones of eastern Kazakhstan: implications from U–Pb detrital zircon ages, geochemistry, and Nd–Hf isotopes. *Int. J. Earth Sci.* <https://doi.org/10.1007/s00531-021-02059-z>.
- Safonova, I., Savinskiy, I., Perfilova, A., Gurova, A., Maruyama, S., Tsujimori, T., 2020. The Itmurundy Pacific-type orogenic belt in northern Balkhash, central Kazakhstan: Revisited plus first U–Pb age, geochemical and Nd isotope data from igneous rocks. *Gondwana Res.* 79, 49–69.
- Safonova, I., Seltmann, R., Kröner, A., Gladkochub, D., Schulmann, K., Xiao, W., Kim, T., Komiya, T., Sun, M., 2011. A new concept of continental construction in the Central Asian Orogenic Belt (compared to actualistic examples from the Western Pacific). *Episodes* 34, 186–194.
- Schmitt, R.S., Fragoso, R.A., Collins, A.S., 2018. Suturing Gondwana in the Cambrian: The Orogenic Events of the Final Amalgamation. In: Siegesmund, S., Basei, M.A. S., Oyhançabal, P., Oriolo, S. (Eds.), *Geology of Southwest Gondwana*. Springer Int. Pub. pp. 411–432.

- Scholl, D.W., von Huene, R., 2007. Crustal recycling at modern subduction zones applied to the past – Issues of growth and preservation of continental basement crust, mantle geochemistry, and supercontinent reconstruction. *Geol. Soc. Am. Mem.* 200, 9–32.
- Shen, P., Pan, H., Seitmuratova, E., Yuan, F., Jakupova, S., 2015. A Cambrian intra-oceanic subduction system in the Bozshakol area, Kazakhstan. *Lithos* 224–225, 61–77.
- Shutov, V.D., 1967. Classification of sandstones. *Lithol. Mineral Resour.* 5, 86–102. in Russian.
- Stepanets, W.G., 2016. Ophiolites of Kazakhstan. *Geology and geodynamics. Acad. Pub. house Lambert.* 251 (in Russian).
- Stern, R., 2010. The anatomy and ontogeny of modern intra-oceanic arc systems. In: Kusky TM, Zhai MG, Xiao W (ed) *The Evolving Continents: Understanding Processes of Continental Growth.* Geol. Soc. London, Spec. Pub. London, 7–34.
- Sun, S., McDonough, W.F., 1989. Chemical and isotopic systematics of oceanic basalts: implications for mantle composition and processes. In: Saunders, A.D., Norry, M.J. (Eds.), *Magmatism in the Ocean Basins.* Geol. Soc. London, Spec. Pub. 42, 313–345.
- Suzuki, K., Maruyama, S., Yamamoto, S., Omori, S., 2010. Have the Japanese Islands grown?: Five “Japan”s were born, and four “Japans” subducted into the mantle. *J. Geograph. (Chigaku Zasshi)* 119, 1173–1196. in Japanese.
- Taylor, S.T., McLennan, S.M., 1985. *The Continental Crust: Composition and Evolution.* Blackwell, Oxford, 312.
- Ueda, H., Kawamura, M., Niida, K., 2000. Accretion and tectonic erosion processes revealed by the mode of occurrence and geochemistry of greenstones in the Cretaceous accretionary complexes of the Itonappu zone, southern central Hokkaido, Japan. *Island Arc* 9, 237–257.
- Wakita, K., 2012. Mappable features of mélanges derived from ocean plate stratigraphy in the Jurassic accretionary complexes of Mino and Chichibu terranes, Southwest Japan. *Tectonophysics* 568–569, 74–85.
- Wakita, K., Metcalfe, I., 2005. Ocean Plate Stratigraphy in East and Southeast Asia. *J. Asian Earth Sci.* 24, 679–702.
- Wang, Y., Wang, B., Li, M., Cao, S., Wang, H., Pan, S., Guo, J., Ma, D., Song, F., Cao, T., Safonova, I.Y., Zhong, L., Ni, X., 2022. New constraints on volcanism during Ordovician-Silurian transition: Insights from marine bentonites in northern Yili Block (NW China). *Palaeogeography, Palaeoclimatology, Palaeoecology* 600, 111073.
- Windley, B.F., Alexeev, D., Xiao, W., Kröner, A., Badarch, G., 2007. Tectonic models for accretion of the Central Asian Orogenic Belt. *J. Geol. Soc. London* 164, 31–47.
- Woodhead, J., Stern, R.J., Pearce, J., Hergt, J., Vervoort, J., 2012. Hf-Nd isotope variation in Mariana Trough basalts: The importance of “ambient mantle” in the interpretation of subduction zone magmas. *Geology* 40 (6), 539–542.
- Wörner, G., Moorbath, S., Harmon, R.S., 1992. Andean Cenozoic volcanic centers reflect basement isotopic domains. *Geology* 20, 1103–1106.
- Xiao, W.J., Huang, B., Han, C., Sun, S., Li, J., 2010. A review of the western part of the Altaids: A key to understanding the architecture of accretionary orogens. *Gondwana Res.* 18, 253–273.
- Xiao, W., Liu, Y., Somerville, I., Schulmann, K., Kusky, T., Seltmann, R., 2020. Accretionary tectonics, deep structures and metallogeny of southern Altaids. *Geol. J.* 55 (3), 1613–1619.
- Xu, Z., Han, B.F., Ren, R., Zhou, Y.Z., Su, L., 2013. Palaeozoic multiphase magmatism at Barleik Mountain, southern West Junggar, Northwest China: Implications for tectonic evolution of the West Junggar. *Int. Geol. Rev.* 55, 633–656.
- Zhang, K.-J., 2004. Secular geochemical variations of the Lower Cretaceous siliciclastic rocks from central Tibet (China) indicate a tectonic transition from continental collision to back-arc rifting. *Earth Planet. Sci. Lett.* 229, 73–89.
- Zheng, R.G., Zhao, L., Yang, Y.Q., 2019. Geochronology, geochemistry and tectonic implications of a new ophiolitic mélange in the northern West Junggar, NW China. *Gondwana Res.* 74, 237–250.
- Zhylykaidarov, A.M., 1998. Conodonts from Ordovician of Central Kazakhstan. *Acta Palaeontol. Pol.* 43, 53–68.
- Zonenshain, L.P., Kuzmin, M.I., Natapov, L.M., 1990. *Geology of the USSR: A Plate Tectonic Synthesis.* Geodynamic Monograph Series. Am. Geophys. Union, Washington. 328 p.